Advances in Water Resources 32 (2009) 885–905

Contents lists available at ScienceDirect

Advances in Water Resources

journal homepage: www.elsevier.com/locate/advwatres

Adaptive Fup multi-resolution approach to flow and advective transport in highly heterogeneous porous media: Methodology, accuracy and convergence

Hrvoje Gotovac [a,b,*], Vladimir Cvetković [a], Roko Andričević [b]

[a] Department of Land and Water Resources Engineering, Royal Institute of Technology, KTH, Brinellvagen 32, SE 10044 Stockholm, Sweden
[b] Department of Civil and Architectural Engineering, University of Split, Matice hrvatske 15, 21000 Split, Croatia

ARTICLE INFO

Article history:
Received 18 May 2008
Received in revised form 24 February 2009
Accepted 25 February 2009
Available online 10 March 2009

Keywords:
Adaptive multi-resolution approach
Flow and advective transport
Highly heterogeneous porous media
Fup basis functions
Monte-Carlo method
Particle tracking

ABSTRACT

In this paper, we present a new Monte-Carlo methodology referred to as Adaptive Fup Monte-Carlo Method (AFMCM) based on compactly supported *Fup* basis functions and a multi-resolution approach. We consider for illustration 2-D steady, linear and unidirectional flow and advective transport defined on a domain of size $64I_Y * 32I_Y$ with isotropic exponential correlation heterogeneity structure and σ_Y^2 up to 8. Accuracy and convergence issues are rigorously analyzed for each realization as well as for the ensemble. Log-conductivity is presented by continuous function at high resolution level ($n_Y = 4$–32 points per integral scale) reproducing very accurately prescribed statistics. The flow problem is the most demanding Monte-Carlo step due to satisfying detailed log-conductivity properties. Presented methodology inherently gives continuous and mesh-free velocity fields, which enables the construction of a new efficient and accurate particle tracking algorithm. Results indicate that resolutions $n_Y = 8$ and $n_h = 32$ enable very accurate flow solutions in each realization with mass balance error less than 3% and accurate ensemble velocity statistics. Results show that the proposed AFMCM enables tracking of an unlimited number of injected particles and calculates required transport variables as continuous functions with desired relative accuracy (0.1%) in each realization. Furthermore, we show that the resolution $n_Y = 8$ yields a quite accurate pdf of the transverse displacement and travel time. All required flow and transport variables require 500 Monte-Carlo realizations in order to stabilize fluctuations of the higher-order moments and the probability density functions.

1. Introduction

Preferential flow channels, nonlinear effects and importance of the higher statistical moments characterize flow and transport in highly heterogeneous porous media. Flow and advective transport in heterogeneous porous media have been analyzed by analytical methods using the small perturbation expansion and the Green's function method (e.g. [12,32,33,47,50]) or spectral techniques (e.g. [3,23,24]). Numerical methods have also been based on single realizations and ergodicity assumption [1,34,60] or on Monte-Carlo (MC) simulations and ensemble averaging [4,10,17,29,30,58].

Perturbation and spectral analytical methods are mainly limited primarily by small variance of the log-conductivity and evaluation of first two statistical moments. Although the MC method is appealing in its conceptual simplicity and generality, capable of producing complete probability density functions (pdf) and all needed higher-order moments, its benefits should be weighted against the large computational efforts typically required. However, the MC is prone to greater or lesser errors which may arise at different stages of the implementation. In particular, when numerically solving flow in highly heterogeneous media, the flow solution with prescribed boundary conditions is a delicate step requiring very fine spatial scales for head and velocity approximations in order to satisfy detailed properties of the highly heterogeneous conductivity field.

The generally accepted conclusion is that there is a good agreement between analytical (perturbation) results and numerical approaches for $\ln K$ variance less than unity. Furthermore, studies have shown an acceptable agreement between analytical and numerical results for mild heterogeneity (σ_Y^2 up to 2), however, there is currently no strong evidence how accurately analytical or MC simulations describe flow and transport in highly heterogeneous porous media ($\sigma_Y^2 > 3$), especially with the commonly assumed exponential correlation structure. Cvetković et al. [10] and Salandin and Fiorotto [58] performed 2-D MC simulations in highly heterogeneous media with the exponential correlation structure for σ_Y^2 up to 4. Recently, de Dreuzy et al. [17] presented powerful parallel 2-D simulations with large domains and σ_Y^2 up to 9,

* Corresponding author. Tel.: +385 21 303 354/+46 8 790 86 90; fax: +385 21 465 117/+46 8 790 86 89.
E-mail addresses: hrvoje.gotovac@gradst.hr, gotovac@kth.se (H. Gotovac), vdc@kth.se (V. Cvetković), rokoand@gradst.hr (R. Andričević).

0309-1708/$ - see front matter © 2009 Elsevier Ltd. All rights reserved.
doi:10.1016/j.advwatres.2009.02.013

however, without strict accuracy or convergence analysis. On the other side, accuracy and convergence analyses were presented only for low and mild heterogeneity (e.g. [52]).

In a three-part series of papers [14,21,34], a general concept for multi-indicator heterogeneity structure [14] and fast semi-analytic algorithm were presented [21], while Janković et al. [34] presented extensive 2-D and 3-D numerical experiments based on one large single realization and analytic element method (σ_Y^2 up to 10 for 2-D and up to 8 for 3-D). Indeed, only Janković et al. [34] provided accurate 3-D numerical simulations in highly heterogeneous porous media to exactly satisfy the flow equation, using powerful supercomputer infrastructure. However, their approach is limited to a multi-indicator heterogeneity structure. The general aim of the present paper is to develop an accurate and robust MC procedure for flow and transport in highly heterogeneous porous media applicable to an arbitrary correlation structure (with finite or infinite $\ln K$ variance) and the possibility to control the error in each step of MC simulations.

Conventional numerical procedures (finite elements, finite volumes and finite differences) are potentially limited for accurately solving problems of flow and transport in highly heterogeneous porous media, and hence new adaptive (e.g. [6,19]), multi-scale finite element (e.g. [7,20,31]), spectral (e.g. [18,57,62]) and meshfree methods (e.g. [2,28,35]) have been proposed as alternatives.

In this paper we are focused on a mesh-free collocation method which uses localized basis functions with compact support such as wavelets and splines (e.g. [49,63–65,67]). Apart from wavelets and splines, there is a relatively lesser known class of atomic or R_{bf} basis functions (Rvachev's basis functions) [53,54]. Atomic functions are classified between classic polynomials and spline functions. However, in practice, their application as basis functions is closer to splines or wavelets. In this study, we shall use *Fup* basis functions which are one type of atomic basis functions (recent reviews in [37,41]). Gotovac and Kozulić [25] systemized the existing knowledge on atomic functions and presented the transformation of basis functions into a numerically applicable form. The application of Fup basis functions has been demonstrated in signal processing [42,68], for solving the integral Fredholm equations [40], in initial value problems [26], and in the non-adaptive collocation method for boundary value problems [27,38]. Recently, the novel Adaptive Fup Collocation Method (AFCM) was developed which is well suited to deal with strong nonlinear groundwater flow and transport problems with sharp fronts and narrow transition zones [28]. Furthermore, this method enables the adaptive multiresolution evolution of a solution (resolving all spatial and temporal scales) with a desired level of accuracy using the entire family of the Fup basis functions.

In this paper we present an accurate and efficient Adaptive Fup Monte-Carlo Method (AFMCM) based on Fup basis functions, Fup transformations and a novel form of the AFCM which is adjusted for complex modeling of flow and transport in highly heterogeneous porous media. We exemplify the method using an exponential correlation structure and $\ln K$ variance up to 8, addressing accuracy and convergence issues. The paper is organized as follows. In the next section, the problem is formulated and the solution methodology outlined. In Section 3, the basis functions, transforms and Monte-Carlo methodology are presented. In Sections 4 and 5, continuous multi-resolution approximation of the conductivity field and AFCM solution of the flow equation are presented, where strict accuracy and convergence analysis are given. Section 6 describes a particle tracking algorithm for particle advection which calculates transport variables such as travel time, transverse displacement and Lagrangian velocity with desired accuracy. Section 7 summarizes discussions with emphasis on new properties of the presented methodology, whereas the last section summarizes the main conclusions.

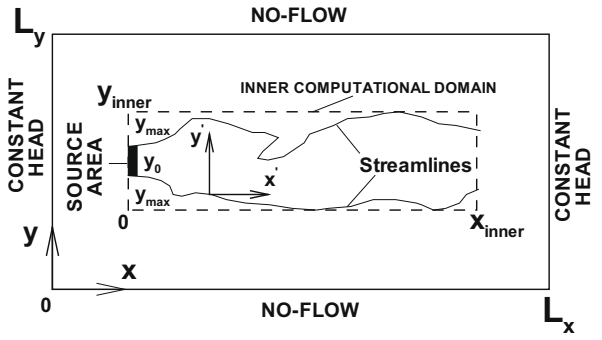

Fig. 1. Simulation domain needed for global flow analysis and inner computational domain needed for flow and transport ensemble statistics.

2. Problem formulation and methodology outline

In this paper we consider single-phase flow and advective transport in heterogeneous porous media using the Eulerian–Lagrangian formulation which separates or decouples flow and transport analysis [12,51]. This physical formulation is common for flow and transport of tracers or contaminants in cases where flow velocity is not significantly influenced by the density differences. Since we are mainly interested to investigate the role of high heterogeneity in flow and advective transport processes, a few additional simplifications will be used. Our first simplification is to consider a two-dimensional and unidirectional flow field with a basic configuration illustrated in Fig. 1. This configuration has been extensively studied in the past (among others [4,29,30,58]) and hence is sufficiently familiar for comparative purpose. The hydraulic conductivity[1] is assumed to be a random space function with specified statistics (mean, variance and correlation length). The second important simplification is that the statistical structure of $\ln K$ will be assumed "classical": multi-Gaussian with an exponential covariance. Note that for numerical simulations of flow with high variances, this "classical" exponential covariance structure poses perhaps the most difficult challenge due to very high spatial gradients in $\ln K$ which need to be captured by numerical algorithms; hence this configuration provides a suitable benchmark for our numerical solution. Finally, we shall limit our present discussion to only one approach for quantifying advective transport: travel time and transverse statistics as functions of the longitudinal distance (i.e. "control plane", parallel to the mean flow, Fig. 1) [9,13].

Fig. 2 shows the flow chart of the proposed Adaptive Fup Monte-Carlo Method (AFMCM) which represents a general framework for flow and advective transport in highly heterogeneous porous media. The methodology is based on Fup basis functions with compact support and a collocation algorithm. AFMCM consists of the following common steps [51]: (1) generation of as high number as possible of equally probable log-conductivity realizations with predefined correlation structure, (2) numerical approximation of the log-conductivity field, (3) numerical solution of the flow equation with prescribed boundary conditions in order to produce head and velocity approximations, (4) evaluation of the displacement position and travel time for a large number of particles, (5) repetition of steps 2–4 for all realizations and (6) statistical evaluation of flow and transport variables such as head, velocity, travel time, transverse displacement, solute flux or concentration (including their cross-moments and pdf's).

We use here the random field generator HYDRO_GEN [5] for generating $\ln K$ fields, due to its accuracy and efficiency (step 1).

[1] We shall refer to "hydraulic conductivity" in spite of the field being 2-D.

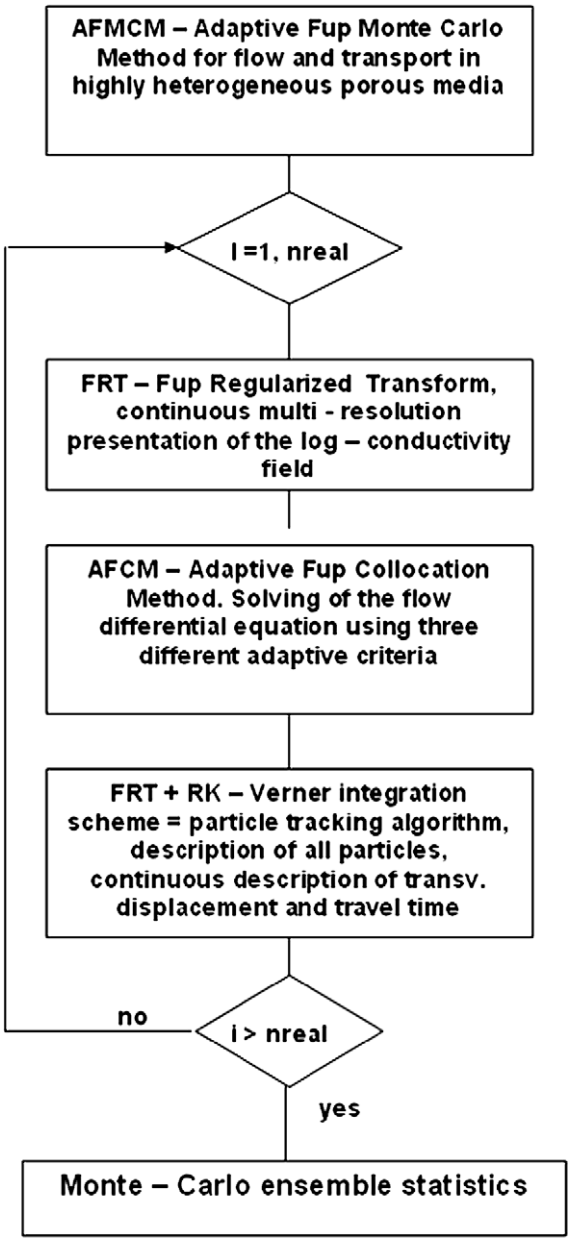

Fig. 2. Flow chart of the presented methodology – AFMCM.

Six discrete values of log-conductivity variance will be considered: 0.25, 1, 2, 4, 6 and 8. In each realization, generated $\ln K$ field is approximated by continuous function which is a linear combination of Fup basis functions (step 2).

Fig. 1 shows a 2-D computational domain ($64I_Y * 32I_Y$) for flow simulations with the corresponding boundary conditions (step 3). In each realization the flow problem is defined by Darcy's Law

$$\mathbf{q}(\mathbf{x}) = -\mathbf{K}(\mathbf{x})\nabla h(\mathbf{x}) \tag{1}$$

and the continuity equation

$$\nabla \cdot \mathbf{q}(\mathbf{x}) = 0 \tag{2}$$

where $\mathbf{q}$ is the Darcy specific discharge (L/T), $\mathbf{K}$ is the conductivity tensor (L/T) and $h(L)$ is the hydraulic head. Combining (1), (2) and assuming isotropic log-conductivity field ($Y = \ln K$) obtained in step 2, a 2-D expanded continuity equation has the final form

$$\frac{\partial^2 h}{\partial x^2} + \frac{\partial^2 h}{\partial y^2} + \frac{\partial Y}{\partial x}\frac{\partial h}{\partial x} + \frac{\partial Y}{\partial y}\frac{\partial h}{\partial y} = 0 \tag{3}$$

The flow is driven by a head difference (Dirichlet fixed boundary conditions), for illustration assumed upstream as $h = h_L$ (left boundary) and downstream as $h = h_R$ (right boundary); Neumann no-flow boundary conditions are prescribed at the top and bottom boundaries (Fig. 1)

$$h(0,y) = h_L; \quad h(L_x,y) = h_R; \quad q_y(x,0) = q_y(x,L_y) = 0 \tag{4}$$

where L_x and L_y are dimensionless lengths of the domain in both directions with respect to the integral scale I_Y. Note that total head drop and hydraulic gradient can be defined by $\Delta H = h_R - h_L$ and $J = \Delta H/L_x$, respectively. In each realization, step 3 includes the solving of the differential flow equation (3) with corresponding boundary conditions (4) for defined log-conductivity function $Y(x,y)$. Final result is the velocity field (Eq. (2); $\mathbf{v} = \mathbf{q}/n_e$ where n_e is the constant effective porosity).

Advective transport is analyzed as pure advection based on the velocity field, following streamlines as particle trajectories (step 4). Particle tracking algorithm implies numerical integration of the following coupled system of ordinary differential equations for each trajectory (e.g. [29]):

$$\frac{dX'}{dt} = v_x(x,y); \quad \frac{dY'}{dt} = v_y(x,y) \tag{5}$$

where $\mathbf{X}(t) = [X'(t), Y'(t)]$ is a Lagrangian displacement vector. The tracer advection trajectory can be described using the Lagrangian position vector as a function of time $\mathbf{X}(t) = [X'(t), Y'(t)]$ which is used in [11], or alternatively, using the travel (residence) time from $x = 0$ to x, $\tau(x)$, and transverse displacement at x, $\eta(x)$ [13]. Formally, τ and η are related to X' and Y' as $\tau(x) = X'^{-1}(x)$ and $\eta(x) = Y'[\tau(x)]$; this description is unique if the tracer moves in the direction of the mean flow only, i.e., if $X'(t)$ is a monotonously increasing function. Therefore, we consider only the first time passages through the control plane. The τ and η are Lagrangian (random) quantities describing advective transport along a streamline. The advective tracer flux $[M/TL]$ is proportional to the joint probability density function (pdf) $f_{\tau\eta}(\tau,\eta;x)$ [10]. Marginal pdfs $f_\tau = \int f_{\tau\eta}\, d\eta$ and $f_\eta = \int f_{\tau\eta}\, d\tau$ separately quantify advective transport in the longitudinal and transverse directions, respectively. It may be noted that in this approach, all Lagrangian quantities depend on space rather than time as in the traditional Lagrangian approach (e.g. [12,59]).

Transport simulations will be performed in the inner domain in order to avoid non-stationary influence of the flow boundary conditions. Particular analysis shows that inner domain of $40I_Y \cdot 16I_Y$ is sufficient to obtain stationary velocity statistics in such a way that inner boundaries are removed for $12I_Y$ and $8I_Y$ in horizontal and vertical directions, respectively (Fig. 1). Source area (or line; $y_0 = 12I_Y$) is represented by the central segment in the left side of the inner transport domain. For this analysis, we consider tracer particles injected in the flux within the source line [15]. Tracer particles injected instantaneously along the source line are followed downstream and the travel time and transverse displacement are monitored at arbitrary control planes at x.

In the sequel we will present all MC methodology components: (a) Fup basis functions and generally atomic basis functions, (b) Fup Collocation Transform (FCT) for data or function approximation, (c) Fup Regularized Transform (FRT) for data or function approximation in the same multi-resolution way as FCT, but computationally more efficient, (d) novel form of the Adaptive Fup Collocation method (AFCM) for approximation of the differential equations and (e) MC statistics represented by Fup basis functions.

In summary, AFMCM uses a random field generator for step 1, FCT or FRT for log-conductivity approximation (step 2), AFCM for the differential flow equation (step 3), particle tracking algorithm for transport approximations based on Runge–Kutta–Verner explicit integration scheme [66] and FRT for step 4 and statistical properties of the Fup basis functions for step 6 (Fig. 2).

3. Basis functions, transformations and Monte-Carlo computations

3.1. Fup basis functions

Atomic basis functions are compactly supported and infinitely differentiable functions [53,54]. Atomic functions, $y(.)$, are defined as solutions of differential–functional equations of the following type:

$$Ly(x) = \lambda \sum_{k=1}^{M} C_k y(ax - b_k) \tag{6}$$

where L is a linear differential operator with constant coefficients, λ is a scalar different than zero, C_k are coefficients of the linear combination, $a > 1$ is a parameter defining the length of the compact support and b_k are coefficients which determine displacements of basis functions. Rvachev and Rvachev [53] in their pioneer work called these basis functions as "atomic" one because they span vector spaces of all three fundamental functions in mathematics: algebraic, exponential and trigonometric polynomials. Also, atomic functions can be divided to the infinite number of small pieces which maintain all their properties implying so called "atomic structure".

The simplest function, which is the most studied among atomic basis functions, is the $up(x)$ function. Function $up(x)$ is a smooth function with compact support $[-1,1]$, which is obtained as a solution of a differential–functional equation:

$$\dot{up}'(x) = 2up(2x+1) - 2up(2x-1) \tag{7}$$

with the normalized condition $\int_{-\infty}^{\infty} up(x)\,dx = \int_{-1}^{1} up(x)\,dx = 1$. Function $up(x)$ can be expressed as an inverse Fourier transform:

$$up(x) = \frac{1}{2\pi}\int_{-\infty}^{\infty} e^{itx} \prod_{j=1}^{\infty} \left(\frac{\sin(t2^{-j})}{t2^{-j}} \right) dt \tag{8}$$

Since Eq. (8) represents the exact, but not mathematically tractable expression, Rvachev [54] and Gotovac and Kozulic [25] provided tractable means for calculating function $up(x)$:

$$up(x) = 1 - \sum_{k=1}^{\infty} (-1)^{1+p_1+\cdots+p_k} p_k \sum_{j=0}^{k} C_{jk}(x - 0, p_1 \cdots p_k)^j \tag{9}$$

where coefficients C_{jk} are rational numbers determined according to the following expression:

$$C_{jk} = \frac{1}{j!} 2^{j(j+1)/2} up(-1 + 2^{-(k-j)}); \quad j = 0,1,\ldots,k,\ k = 1,2,\ldots,\infty \tag{10}$$

Calculation of the $up(-1+2^{-r})$; $r \in [0,\infty]$ in binary-rational points (Eq. (10)), as well as all details regarding the calculation of the function $up(x)$ values, is provided in [25,26]. The argument $(x - 0, p_1 \cdots p_k)$ in Eq. (9) is the difference between the real value of coordinate x and its binary form with k bits, where $p_1 \cdots p_k$ are digits, 0 or 1, of the binary development of the coordinate x value. Therefore, the accuracy of the coordinate x computation and, thus, the accuracy of the $up(x)$ function at an arbitrary point, depends on machine accuracy.

From Eq. (7) it can be seen that the derivatives of the $up(x)$ function can be calculated simply from the values of the function itself. The general expression for the derivative of the mth degree is:

$$up^{(m)}(x) = 2^{C_{m+1}^2} \sum_{k=1}^{2^m} \delta_k up(2^m x + 2^m + 1 - 2k), \quad m \in N \tag{11}$$

where $C_{m+1}^2 = m(m+1)/2$ is the binomial coefficient and δ_k are the coefficients with ±1 value according to the recursive formulas $\delta_{2k-1} = \delta_k$, $\delta_{2k} = -\delta_k$, $k \in N$, $\delta_1 = 1$. It can be observed that the derivatives consist of the $up(x)$ function compressed to the interval of 2^{-m+1} length with ordinates "extended" with the $2^{C_{m+1}^2}$ factor.

The $Fup_n(x)$ function satisfies the following differential–functional equation:

$$\dot{Fup}_n'(x) = 2\sum_{k=0}^{n+2} (C_{n+1}^k - C_{n+1}^{k-1}) \dot{Fup}_n(x)(2x - 2^{-n-1}k + 2^{-n-2}(n+2)) \tag{12}$$

where n is the Fup order. For $n = 0$, $Fup_0(x) = up(x)$, since $Fup_n(x)$ and its derivatives can be calculated using a linear combination of displaced $up(x)$ functions instead of using their Fourier transforms:

$$Fup_n(x) = \sum_{k=0}^{\infty} C_k^*(n) up\left(x - 1 - \frac{k}{2^n} + \frac{n+2}{2^{n+1}} \right) \tag{13}$$

where $C_0^*(n) = 2^{C_{n+1}^2} = 2^{n(n+1)/2}$ and $C_k^*(n) = C_0^*(n) \cdot C_k'(n)$, where a recursive formula is used for calculating auxiliary coefficients $C_k'(n)$:

$$\begin{aligned} &C_0'(n) = 1, \quad \text{when } k = 0;\ \text{i.e. when } k > 0 \\ &C_k'(n) = (-1)^k C_{n+1}^k - \sum_{j=1}^{\min\{k;2^{n+1}-1\}} C_{k-j}'(n) \cdot \delta_{j+1} \end{aligned} \tag{14}$$

The $Fup_n(x)$ is defined on the compact support $[-(n+2)2^{-n-1}, (n+2)2^{-n-1}]$. Fig. 3 shows the $Fup_2(x)$ function and its first two derivatives which are used in this paper.

Index n also denotes the highest degree of the polynomial which can be expressed exactly in the form of a linear combination of $n+2$ $Fup_n(x)$ basis functions displaced by a characteristic interval 2^{-n}. Thus, a quadratic polynomial on a characteristic interval 2^{-n} can be exactly presented in the following way:

$$x^2 = 2^{-6} \sum_{k=-1}^{2} (k^2 - 5/18) Fup_2(x - k/4) \tag{15}$$

Fup basis functions, wavelets and splines are similar mainly due to the compact support and possible numerical implementation. Generally, approximation properties of all these basis functions are related to the developing of algebraic polynomials. *Fup* and other atomic basis functions can be regarded as generalized splines of infinite smoothness (C^∞). It is a reason why Fourier transform of

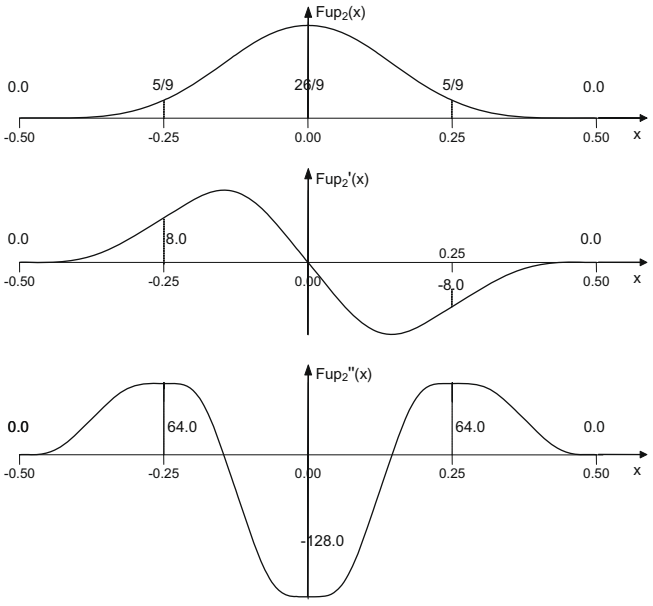

Fig. 3. Function $Fup_2(x)$ and its first two derivatives.

$up(x)$ can be obtained by infinite number of convolution (Eq. (8)). In the spirit of wavelet and multi-resolution analysis, atomic basis functions can be regarded as scaling functions which enable a direct relationship with wavelets [44]. Therefore, Kolodyazhny and Rvachev [36] and Kravchenko and Rvachev [39] constructed wavelet systems using the atomic functions. It should be noted that the importance of the atomic function $up(x)$ in the functional–theoretical sense follows from its "atomic role" in the space of C^∞ functions that is similar to that played by wavelet functions in the space $L^2(R)$. Also, the relation between the $up(x)$ function and the theory of wavelet functions is shown in [16].

The basic difference between *Fup* and atomic basis functions on the one hand and wavelets and splines on the other hand is that, generally, atomic basis functions presented exact solutions of differential–functional equations, but splines and wavelets are obtained from particular types of mathematical transforms. This is the reason why *Fup* basis functions have infinite number of derivatives and non-vanishing moments. Therefore, *Fup* and atomic basis functions are appropriate for a efficient solving of the boundary-initial value problems as well as designing new promising mesh-free numerical approaches. A more detailed discussion about Fup and atomic basis functions is given in Gotovac and Kozulic [25] as well as in recent reviews of atomic basis functions and its application [37,41].

3.2. Fup Collocation Transform (FCT)

The Fup Collocation Transform (FCT) is an efficient numerical tool for describing various types of data, signals and functions using a linear combination of the Fup basis functions. It is a discrete type of transform, similar to the classic discrete Fourier transform (DFT), where linear combination coefficients are called Fup coefficients. However, the main disadvantage of DFT lies in the fact that unresolved locations of important frequencies have not been defined due to non-localized properties of classic trigonometric basis functions. Thus, the presented transform based on the Fup basis functions with a compact support (Fig. 3) enables that specific frequencies and corresponding Fup coefficients are associated with a particular resolution level and spatial location which is not possible in the DFT. This procedure is also known as a multi-resolution analysis commonly linked with wavelets [44]. The transform is obtained through a collocation procedure and is therefore called the Fup Collocation Transform [28]. For example, the 1-D multi-resolution expansion of the $u(x)$ function can be expressed in the following way:

$$u^J(x) = \sum_{j=0}^{J} \sum_{k=-n/2}^{(2^{j_{\min}+j}+n/2)} d_k^j \varphi_k^j(x); \quad J \in [0,\infty) \tag{16}$$

where j is the resolution level, from zero to a maximum level J, needed for the Fup presentation in Eq. (16) with desired accuracy defined by the threshold ε, n is the Fup order, $j_{\min}$ is the resolution at the zero level, d_k^j are Fup coefficients, φ_k^j are Fup basis functions and k denotes the location index at the current level. If we define the domain $\Omega = [X_1, X_2]$, then the characteristic interval at each level is equal to the scale or distance between adjacent collocation points: $\Delta x_j = (X_2 - X_1)/2^{j_{\min}+j}$. For demonstrating FCT, consider the following 1-D test function:

$$f(x) = -\tanh\left(\frac{x - 2/3}{0.02}\right) \tag{17}$$

with a chosen high threshold of $\varepsilon = 0.07$ for illustrative purposes. Other parameters are $j_{\min} = 2$, $X_1 = 0$, $X_2 = 2$ and $n = 4$. Fig. 4 presents the adaptive multi-resolution Fup Collocation Transform for a chosen function (Eq. (17)).

Basis functions are characterized by vertices (Fig. 4a). Basis functions whose vertices are located inside the domain are called internal basis functions. Other functions are external basis functions and only their influence within the domain is considered. The best choice for the location of the collocation points is vertices of the internal basis functions as proven numerically for splines in [49], wavelets in [63] and Fup basis functions in [25]. Moreover, the main difficulty in transformations with localized basis functions is the special treatment of the boundary. For all $n/2$ external basis functions at the left and right boundaries, the collocation points are located at the X_1 and X_2 boundaries if n is the *Fup* order. The location of each basis function is actually determined by the location of the vertex and defined by $b_k^j = X_1 + k\Delta x_j$. The calculation of basis function values and their derivatives at a general characteristic interval Δx_j should be done in the following form with respect to a basic characteristic interval 2^{-n}:

$$\varphi_k^{j\,(m)}(x) = \frac{1}{(2^n \Delta x_j)^{(m)}} Fup_n^{(m)}\left(\frac{x - b_k^j}{2^n \Delta x_j}\right) \tag{18}$$

where m is the order of the derivative. The compact support of the basis function at every level has $(n+2)\Delta x_j$ length.

Fig. 4a shows an adaptive grid for all levels and internal basis functions for the zero and first levels. Each next level includes two times more internal basis functions with two times less support and scale. Zero level is the starting (coarsest) level which is always present in the grid. The FCT satisfies function values in all collocation points and for the first two $(n/2)$ derivatives at boundary points (Fig. 4b). The key step of the FCT is the transfer from the current level to the next level. The residual between the true function and the previous level approximation is checked and the points with a residual below the prescribed threshold are dropped from the grid (Fig. 4c). This procedure presents an a priori adaptive criterion for defining the new collocation points at the next level. Note that residuals are always zero for even collocation points due to satisfying function values at the previous levels. Each retained point must be surrounded by $n+2$ additional basis functions which enable a consistent approximation for the transfer to the next level. In addition, external basis functions should be added if points near the boundary are present in the grid.

For the first and for each subsequent level the collocation algorithm should only satisfy the residual between the true function and its approximation from the previous levels. In other words, all Fup coefficients from the previous levels are "frozen" and only Fup coefficients at the current level should be solved. Higher levels include only higher frequencies and show a more detailed description of the chosen function. The collocation points are added only around the front where the residual from the previous level is greater than the prescribed threshold (Fig. 4a and c). Finally, the residual between true function and its *Fup* approximation up to five levels is less than the threshold within the entire domain. In this way, we can decompose any function in a multi-resolution fashion by employing only a few significant Fup basis functions with appropriate scales (frequencies) and locations with a desired level of accuracy and a near minimum computational cost. Finally, the meaning of the threshold is twofold: (1) it presents a priori adaptive criterion and (2) it defines the accuracy of the approximation because the final absolute difference between the Fup approximation and the real function must be less than the threshold.

Extension of the FCT to higher dimensions is the straightforward task. Multi-dimensional basis functions are obtained by Cartesian product of the 1-D basis functions (Fig. 3). The multi-resolution 2-D FCT of the function $u(x,y)$ can be presented in the following way:

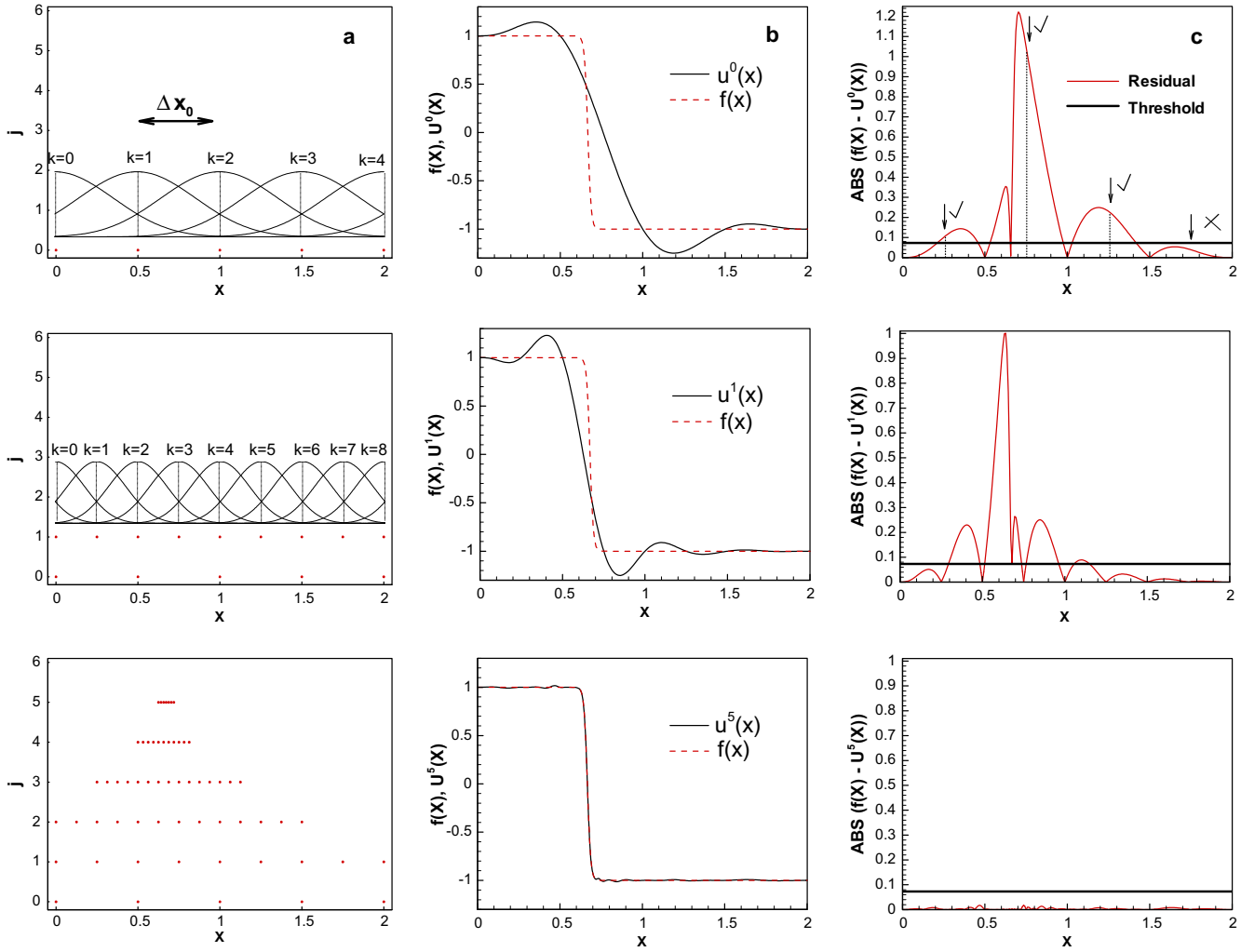

Fig. 4. Multi-resolution approximation of the function (17), (a) adaptive grid development and internal basis functions, (b) function (17) and its FCT approximation and (c) a priori adaptive criterion for new collocation points based on residual between function (17) and its FCT approximation.

$$u^J(x,y)=\sum_{j=0}^{J}\sum_{k,l\in Z^j} d_{k,l}^j\varphi_{k,l}^j(x,y) \tag{19}$$

where Z^j is the irregular grid at each level which contains only the significant collocation points and *Fup* basis functions needed for the *Fup* presentation in Eq. (19) with desired accuracy defined by the threshold ε, $d_{k,l}^j$ are *Fup* coefficients, $\varphi_{k,l}^j$ are *Fup* basis functions while k and l presents the indexes of collocation points at the current level for x- and y-direction, respectively. The zero level is defined by a chosen resolution level $j_{\min x}$ for the x-direction and by $j_{\min y}$ for the y-direction. Generally, a sparse linear system of equations can be obtained at each level:

$$\sum_{k,l\in Z^j} d_{k,l}^j\varphi_{k,l}^j(x_p^j,y_q^j)=\Delta_j(x_p^j,y_q^j),\quad p,\ q\in Z^j:0\leqslant p\leqslant 2^{j_{\min x}+j},\ 0\leqslant q\leqslant 2^{j_{\min y}+j} \tag{20}$$

$$\sum_{k,l\in Z^j} d_{k,l}^j\varphi_{k,l}^{j\,(m_x,m_y)}(x_p^j,y_q^j)=\Delta_j^{(m_x,m_y)}(x_p^j,y_q^j),\quad p,\ q\in Z^j:(p=0 \text{ or } p=2^{j_{\min x}+j} \text{ or } q=0 \text{ or } q=2^{j_{\min y}+j}) \text{ and } (m_x>0 \text{ or } m_y>0) \tag{21}$$

where m_x and m_y are orders of the derivative in x and y directions, respectively. System (20)–(21) presents conditions for satisfying function values within the domain (Eq. (20)) and partial derivatives at the boundary points (Eq. (21)). Boundary conditions satisfy the smallest order of the derivatives if the function is known or neglect the highest possible order of the derivatives (up to the *Fup* order) if the function is unknown or defined as set of data (i.e. log-conductivity). The residual vector has the following form:

$$\Delta_j(x_p^j,y_q^j)=\begin{cases} f(x_p^j,y_q^j), & p,\ q\in Z^j;\ j=0\\ f(x_p^j,y_q^j)-u^{j-1}(x_p^j,y_q^j), & p,\ q\in Z^j;\ j>0\end{cases}$$

$$\Delta_j^{(m_x,m_y)}(x_p^j,y_q^j)=\begin{cases} f^{(m_x,m_y)}(x_p^j,y_q^j), & p,\ q\in Z^j;\ j=0\\ f^{(m_x,m_y)}(x_p^j,y_q^j)-u^{j-1\,(m_x,m_y)}(x_p^j,y_q^j), & p,\ q\in Z^j;\ j>0\end{cases} \tag{22}$$

More detailed description of the FCT is given in Gotovac et al. [28]. Accuracy of the FCT is given by Theorems 1 and 2 which hold true for each direction (Appendix A). Kravchenko and Basarab [40] proposed iteration algorithm for solving the system (20)–(21) as modified type of the classic Jacobi iterative procedure:

$$d_{k,l,s}^j=2^{-n}\sum_{i=0}^{s}\left(1-\sum_{p=0}^{n/2}a_{x,p}\Delta_x^{2p}\sum_{q=0}^{n/2}a_{y,q}\Delta_y^{2q}\right)^i u(x_k^j,y_l^j) \tag{23}$$

where s is the number of iterations, Δ_x and Δ_y are finite difference operators of even order with respect to each direction and

$a_{x,n/2} = \varphi_k^j(b_{k-n/2}^j)$; $a_{x,n/2-r} = \varphi_k^j(b_{k-n/2+r}^j) + \sum_{i=1}^{r}(-1)^{i+1}C_{2(n/2-r+i)}^i$ $a_{x,n/2-r+i}$, $r = 1,\ldots,n/2$ for x-direction and consequently $a_{y,q}$ for y-direction. By letting $s \to \infty$, we obtain the exact solution of the system (20)–(21). However, for a prescribed threshold it is possible to obtain sufficient number of iterations in order to get an approximate solution of the system (20)–(21).

3.3. Fup Regularized Transform (FRT)

The Fup Regularized Transform (FRT) is a numerical tool for describing various types of data, signals and functions using a linear combination of the Fup basis functions as well as FCT, but in a computationally more efficient way. The main drawback of the FCT is solving of the sparse linear system of equations at each level (20)–(21). Although there are a few efficient solvers including Eq. (23), generally for higher Fup basis functions, adaptive grids and especially 3-D problems, solving of the mentioned system can be a very demanding. Here, we present for the first time the Fup Regularized Transform (FRT) which directly connects function or data values with Fup coefficients without solving the system of equations. Generally, FRT has the same purpose and uses the complete same adaptive strategy as FCT and therefore we will focus only on obtaining the *Fup* coefficients.

Without loss of generality, we can demonstrate FRT on a very simple 1-D function approximation with Fup_2 basis functions. For equidistant distribution of function values at some level j, we can calculate few first derivatives in some point x_k^j using the classic Taylor expansion. For Fup_2 basis functions ($n = 2$) only three points ($n + 1 = 3$) are needed in order to obtain the well known central difference formulas:

$$\begin{bmatrix} u_k^j \\ u_k^{j(1)} \\ u_k^{j(2)} \end{bmatrix} = \begin{bmatrix} 0 & 1 & 0 \\ \frac{-1}{2\Delta x_j} & 0 & \frac{1}{2\Delta x_j} \\ \frac{1}{\Delta x_j^2} & \frac{-2}{\Delta x_j^2} & \frac{1}{\Delta x_j^2} \end{bmatrix} \begin{bmatrix} u_{k-1}^j \\ u_k^j \\ u_{k+1}^j \end{bmatrix} \tag{24}$$

On the other side, Fup expansion of the function value and first two derivatives at the same point are defined by (Eqs. (13) and (18), Fig. 3):

$$\begin{bmatrix} u_k^j \\ u_k^{j(1)} \\ u_k^{j(2)} \end{bmatrix} = \begin{bmatrix} \frac{5}{9} & \frac{26}{9} & \frac{5}{9} \\ \frac{-2}{\Delta x_j} & 0 & \frac{2}{\Delta x_j} \\ \frac{4}{\Delta x_j^2} & \frac{-8}{\Delta x_j^2} & \frac{4}{\Delta x_j^2} \end{bmatrix} \begin{bmatrix} d_{k-1}^j \\ d_k^j \\ d_{k+1}^j \end{bmatrix} \tag{25}$$

Equalizing (24) and (25) will give the Fup coefficient at point x_k^j:

$$d_k^j = \frac{1}{144}\begin{bmatrix} -5 & 46 & -5 \end{bmatrix} \begin{bmatrix} u_{k-1}^j \\ u_k^j \\ u_{k+1}^j \end{bmatrix} \tag{26}$$

External and corresponding internal Fup coefficients should be obtained from the closest neighboring points to the boundary collocation point using the backward or upward FD formulas. For example, at left boundary (X_1) the *Fup* coefficients are:

$$\begin{bmatrix} d_{-1}^j \\ d_0^j \end{bmatrix} = \frac{1}{144}\begin{bmatrix} 103 & -98 & 31 \\ 31 & 10 & -5 \end{bmatrix} \begin{bmatrix} u_0^j \\ u_1^j \\ u_2^j \end{bmatrix} \tag{27}$$

In other words, FCT exactly satisfies function values, while FRT locally at each collocation point describes a function using equivalence between Fup and polynomial approximation. Therefore, FRT exactly describes polynomials up to the *Fup* order. Note that evaluation of the FRT to higher dimensions and *Fup* basis functions is a straightforward task because it is only necessary to equalize corresponding Fup expansion and finite difference formulas. If we calculate all Fup coefficients (Eqs. (25) and (26)) at level j, then Eq. (16) at point x_k^j does not give exact function value as FCT and it can be presented with respect to the only function values:

$$u^j(x_k^j) = \frac{1}{1296}\begin{bmatrix} -25 & 100 & 1146 & 100 & -25 \end{bmatrix} \begin{bmatrix} u_{k-2}^j \\ u_{k-1}^j \\ u_k^j \\ u_{k+1}^j \\ u_{k+2}^j \end{bmatrix} \tag{28}$$

Therefore, FRT approximation (28) can be interpreted as regularization because it uses closest points with corresponding weighting factors the total sum of which is unity [12]. Since FCT and FRT exactly describe polynomials up to the *Fup* or n-order, Kravchenko and Basarab [40] showed that Eq. (23) also presents n-order polynomials if $s = n/2$. It means that the general expression for FRT is given by

$$u_n^J(x,y) = \sum_{j=0}^{J}\sum_{k,l\in Z^j} d_{k,l,n/2}^j \varphi_{k,l}^j(x,y) \tag{29}$$

Difference between the FCT and FRT approximation is defined by Theorem 3 in Appendix A. FCT requires slightly less number of collocation points than FRT for a general function. However, FRT is computationally more efficient due to the direct connection of the Fup coefficients and function values while still maintaining good approximation properties (Appendix A). In this paper we use FRT for all 1-D and 2-D data or function approximations as well as for ensemble statistics.

3.4. Adaptive Fup Collocation Method (AFCM)

In this paper, we present a novel form of the Adaptive Fup Collocation Method (AFCM) which solves the flow differential equation with only Fup basis functions at each level using the collocation framework. All previous existing algorithms with wavelets and splines (e.g. [63–65,67]) as well as the recent form of AFCM [28] used localized basis functions only to obtain an efficient adaptive strategy, but the differential equation is solved by finite difference method on a non-uniform adaptive grid (including all levels). Essentially, AFCM which solves the differential flow equation and corresponding boundary conditions (3) and (4) uses the same adaptive strategy as FCT and approximates a head solution by levels. Zero level satisfies boundary conditions and flow equation in the corresponding collocation points. Each non-zero level solves only residual of the flow equation and corresponding boundary conditions from all previous levels (“frozen” *Fup* coefficients) and gives particular head correction (*Fup* coefficients at the current level). Adaptive criterion adds new collocation points in the next level only in the zones where head correction is greater than the prescribed threshold. Additional and external basis functions and collocation points are added in the same way as it is shown in the FCT or FRT.

Many numerical experiments with known analytic solutions [27,38] have shown that solution (head) correction on some level is greater than the difference between the analytical solution and overall solution up to that level. This implies that head correction is a priori an adaptive criterion, which directly estimates accuracy of the solution even if the analytical solution is not a priori known. Numerical AFCM implementation of the flow problem (3) and (4) can be represented by the following linear and sparse system of equations at each level:

$$\sum_{k,l\in Z^j} d^j_{k,l}\left(\frac{\partial^2\varphi^j_{k,l}(x^j_p,y^j_q)}{\partial x^2}+\frac{\partial^2\varphi^j_{k,l}(x^j_p,y^j_q)}{\partial y^2}\right)+\frac{\partial Y(x^j_p,y^j_q)}{\partial x}\left(\sum_{k,l\in Z^j} d^j_{k,l}\frac{\partial\varphi^j_{k,l}(x^j_p,y^j_q)}{\partial x}\right)+\frac{\partial Y(x^j_p,y^j_q)}{\partial y}\left(\sum_{k,l\in Z^j} d^j_{k,l}\frac{\partial\varphi^j_{k,l}(x^j_p,y^j_q)}{\partial y}\right)=\Delta_j(x^j_p,y^j_q):0\leqslant p\leqslant 2^{j_{\min x}+j},\ 0\leqslant q\leqslant 2^{j_{\min y}+j},\ p,\ q\in Z^j \tag{30}$$

with boundary conditions:

$$\sum_{k,l\in Z^j} d^j_{k,l}\varphi^j_{k,l}(x^j_p,y^j_q)=\Delta^{(n_x,n_y)}_j(x^j_p,y^j_q):(p=0\text{ or }p=2^{j_{\min x}+j},\ p,\ q\in Z^j) \tag{31}$$

$$\sum_{k,l\in Z^j} d^j_{k,l}\frac{\partial\varphi^j_{k,l}(x^j_p,y^j_q)}{\partial y}=\Delta^{(n_x,n_y)}_j(x^j_p,y^j_q):(q=0\text{ or }q=2^{j_{\min y}+j},\ p,\ q\in Z^j) \tag{32}$$

for a given FCT or FRT approximation of the log-conductivity field, while n_x and n_y are absolute differences between indexes of the vertices of the external basis functions and corresponding boundary collocation points in x and y directions, respectively [28]. System (30)–(32) satisfies the differential flow equation in the internal collocation points (internal Fup coefficients) and boundary conditions in the corresponding boundary collocation points (external Fup coefficients). The residual vector has the following form:

$$\begin{aligned}&\Delta_j(x^j_p,y^j_q)=0:0\leqslant p\leqslant 2^{j_{\min x}+j},\ 0\leqslant q\leqslant 2^{j_{\min y}+j},\ p,\ q\in Z^j;\ j=0\\&\Delta_j(x^j_p,y^j_q)=0-\sum_{i=0}^{j-1}\left[\sum_{k,l\in Z^i} d^i_{k,l}\left(\frac{\partial^2\varphi^i_{k,l}(x^j_p,y^j_q)}{\partial x^2}+\frac{\partial^2\varphi^i_{k,l}(x^j_p,y^j_q)}{\partial y^2}\right)+\frac{\partial Y(x^j_p,y^j_q)}{\partial x}\left(\sum_{k,l\in Z^i} d^i_{k,l}\frac{\partial\varphi^i_{k,l}(x^j_p,y^j_q)}{\partial x}\right)+\frac{\partial Y(x^j_p,y^j_q)}{\partial y}\left(\sum_{k,l\in Z^i} d^i_{k,l}\frac{\partial\varphi^i_{k,l}(x^j_p,y^j_q)}{\partial y}\right)\right]:\\&0\leqslant p\leqslant 2^{j_{\min x}+j},\ 0\leqslant q\leqslant 2^{j_{\min y}+j},\ p,\ q\in Z^j;\ j>0\end{aligned} \tag{33}$$

$$\begin{aligned}&\Delta^{(n_x,n_y)}_j(x^j_p,y^j_q)=h_L:(p=0,\ p,\ q\in Z^j);\ j=0\\&\Delta^{(n_x n_y)}_j(x^j_p,y^j_q)=h_L-\sum_{i=0}^{j-1}\sum_{k,l\in Z^i} d^i_{k,l}\varphi^i_{k,l}(x^j_p,y^j_q):\\&(p=0,\ p,\ q\in Z^j);\ j>0\end{aligned} \tag{34}$$

$$\begin{aligned}&\Delta^{(n_x,n_y)}_j(x^j_p,y^j_q)=h_R:(p=2^{j_{\min x}+j},\ p,\ q\in Z^j);\ j=0\\&\Delta^{(n_x,n_y)}_j(x^j_p,y^j_q)=h_R-\sum_{i=0}^{j-1}\sum_{k,l\in Z^i} d^i_{k,l}\varphi^i_{k,l}(x^j_p,y^j_q):\\&(p=2^{j_{\min x}+j},\ p,\ q\in Z^j);\ j>0\end{aligned} \tag{35}$$

$$\begin{aligned}&\Delta^{(n_x,n_y)}_j(x^j_p,y^j_q)=0:(q=0\text{ or }q=2^{j_{\min y}+j},\ p,\ q\in Z^j);\ j=0\\&\Delta^{(n_x,n_y)}_j(x^j_p,y^j_q)=0-\sum_{i=0}^{j-1}\sum_{k,l\in Z^i} d^i_{k,l}\frac{\partial\varphi^i_{k,l}(x^j_p,y^j_q)}{\partial y}:\\&(q=0\text{ or }q=2^{j_{\min y}+j},\ p,\ q\in Z^j);\ j>0\end{aligned} \tag{36}$$

In this paper we use Fup_2 basis functions. If we wish to use higher Fup order, additional boundary equations should be employed in order to neglect higher possible partial derivatives up to the *Fup* order. System (30)–(32) can be efficiently solved for instance by the GMRES solver, as will be shown in Section 4. Apart from head correction criterion, AFCM uses local grid flow Peclet and global mass balance criteria. Velocity approximation (Eq. (2)) is continuous due to properties of the localized Fup basis functions and continuous FCT or FRT approximation of the log-conductivity. AFCM is generally a mesh-free method because it requires only adding of collocation points and basis functions over the domain, not the classic domain discretization and the numerical integration [2]. In spirit, the Fup multi-resolution approach finds minimum finite number of collocation points or basis functions to represent solution which is theoretically defined by an infinite number of collocation points. The only consequence of this approach is that the exact solution and Fup approximation differ for some non-zero residual, but it is *smaller* than the prescribed threshold.

3.5. Monte-Carlo statistics

Each variable is represented by a separate linear combination of *Fup* basis functions in each realization (Eqs. (16), (19) or (29)). In this subsection we show that ensemble MC averaging also produces a continuous approximation of all flow and transport moments, pdf's or cdf's. Without loss of generality, consider a 1-D case. The mean solution at each point can be obtained in the following way:

$$\langle u(x)\rangle=\sum_{j=0}^{J}\sum_{k\in Z^j}\bar{d}^j_k\varphi^j_k(x) \tag{37}$$

where $\bar{d}^j_k$ are mean Fup coefficients. Eq. (37) implies that the mean solution is presented by mean values of the Fup coefficients. Fup fluctuating coefficients in each realization are defined in the usual way as the difference between actual and mean Fup coefficients ($d^{j\prime}_k=d^j_k-\bar{d}^j_k$). Autocovariance is defined by:

$$\langle u(x_1)'u(x_2)'\rangle=\sum_{i=0}^{J}\sum_{j=0}^{J}\sum_{k\in Z^i}\sum_{l\in Z^j} d^{i\prime}_k d^{j\prime}_l\varphi^i_k(x_1)\varphi^j_l(x_2) \tag{38}$$

Autocovariance (38) is presented by the covariance of the *Fup* fluctuating coefficients. We can conclude that each moment is a continuous function which is represented by a linear combination of the *Fup* basis functions. Linear coefficients are related to the ensemble statistics of the *Fup* coefficients. Furthermore, in this way the same statistics of the Fup coefficients define statistics of all derivatives of the basic variables. For example, covariance between function u and its first derivative is:

$$\left\langle u(x_1)'\frac{\partial u(x_2)'}{\partial x}\right\rangle=\sum_{i=0}^{J}\sum_{j=0}^{J}\sum_{k\in Z^i}\sum_{l\in Z^j} d^{i\prime}_k d^{j\prime}_l\varphi^i_k(x_1)\frac{\partial\varphi^j_l(x_2)}{\partial x} \tag{39}$$

Note that cross-covariance can be obtained similarly as in (38), but linear coefficients are changed to the cross-covariance of the Fup fluctuating coefficients. A computation of all higher moments and pdf's follows an analogous procedure.

4. Multi-resolution representation of hydraulic properties and groundwater flow

To demonstrate the applicability of AFMCM and study advective transport in highly heterogeneous media, we perform unconditional MC simulations in a two-dimensional heterogeneous field ($64I_Y * 32I_Y$) with a log-normally distributed multi-Gaussian hydraulic conductivity, exponential correlation structure and a

ln$K$ variance of hydraulic conductivity, σ_Y^2, up to 8. In the simulations, 4–32 collocation points per integral scale ($n_Y = 4$–32) will be considered.

4.1. Hydraulic properties

A single realization of the hydraulic conductivity obtained using HYDRO_GEN [5] is illustrated in Fig. 5. A discrete set of generated log-conductivity values are transformed to the continuous function by the Fup Collocation Transform (FCT). FCT satisfies exactly generated grid values and elsewhere interpolation is closely related to the polynomial approximation of the n order if n is a *Fup* order (we use here Fup_2 basis functions). Fig. 5 shows a multi-resolution FCT approximation of the log-conductivity field in one chosen realization for $\sigma_Y^2 = 6$. HYDRO_GEN generates 32 grid values per integral scale with conductivity differences over seven orders of magnitude. Zero level satisfies minimum requirement of two collocation points per integral scale ($n_Y = 2$). First level is two times denser, 4 points per integral scale ($n_Y = 4$, Fig. 5a), while second, third and fourth levels consist of $n_Y = 8$, 16 and 32 (Fig. 5b) collocation points per integral scale, respectively. Final, fourth level exactly reproduces all HYDRO_GEN values, but interestingly visual inspection does not reveal any difference between the first and fourth levels. However, in cross-section A–A (Fig. 5c) we see that differences between different resolution levels exist only at higher level points.

Accuracy of the HYDRO_GEN and FCT is shown on Fig. 6 for 500 MC realizations and $\sigma_Y^2 = 6$. Prescribed and reproduced correlations (Fig. 6a) and distributions (Fig. 6b) are practically identical. FCT has some important properties: (1) approximation does not change HYDRO_GEN statistics (by comparison, Ababou et al. [1] and Salandin and Fiorotto [58] reported that ln$K$ variance is distorted around 10%), (2) log-conductivity is a continuous function with all n continuous derivatives if n is a *Fup* order which is contrary to the classical finite element (FE) algorithms where it is usually piecewise constant or a discontinuous function, (3) log-conductivity can be presented at the generated HYDRO_GEN level (Fig. 5b, $n_Y = 32$), but also at all coarser levels (i.e. $n_Y = 4$, 8 and 16 points, Fig. 5a and c) due to the multi-resolution nature of the FCT, (4) MC statistics, for instance log-conductivity correlation and the probability density function (pdf) (Fig. 6), are obtained as continuous functions and (5) not limited to the type of the heterogeneity structure.

On the other side, FRT slightly modifies HYDRO_GEN statistics due to averaging and regularization of the generated values. Fig. 6a shows that FRT actually does not significantly change the correlation structure, but slightly decreases ln$K$ variance and modifies the log-normal distribution close to the origin (Fig. 6b). Therefore, ln$K$ variance is 3–4% reduced for the high heterogeneity cases ($\sigma_Y^2 = 6$—8), but for smaller σ_Y^2 differences are negligible. Although FCT exactly reproduces log-conductivity ensemble statistics, we choose FRT in this paper due to its computational efficiency and comparatively high accuracy. Note that FRT retains all aforementioned properties of the FCT and also shows significant advantage due to more stabilized flow solver and particle tracking algorithm as will be shown in the sequel.

4.2. Groundwater flow

AFCM yields multi-resolution solution of the flow equation resolving different spatial heterogeneity scales (Section 3.5). This method can estimate head and mass balance errors. Each variable

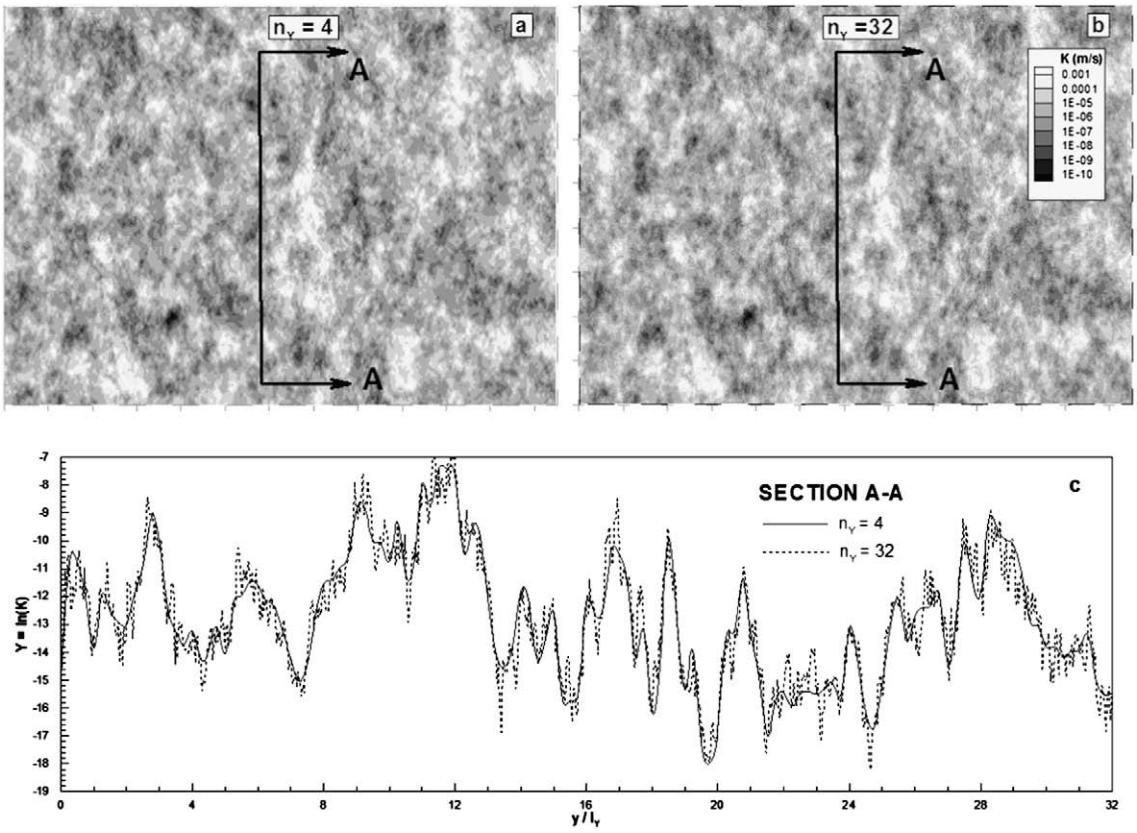

Fig. 5. Multi-resolution Fup approximation of the (log)-conductivity field (one chosen multi-Gaussian realization) obtained by FCT with exponential covariance and $\sigma_Y^2 = 6$ for different resolution levels (domain is $64 l_Y * 32 l_Y$): (a) conductivity field for $n_Y = 4$; $j = 1$, (b) conductivity field for $n_Y = 32$; $j = 4$ which is also HYDRO_GEN resolution level and (c) log-conductivity field for section A–A, $n_Y = 4$ and $n_Y = 32$.

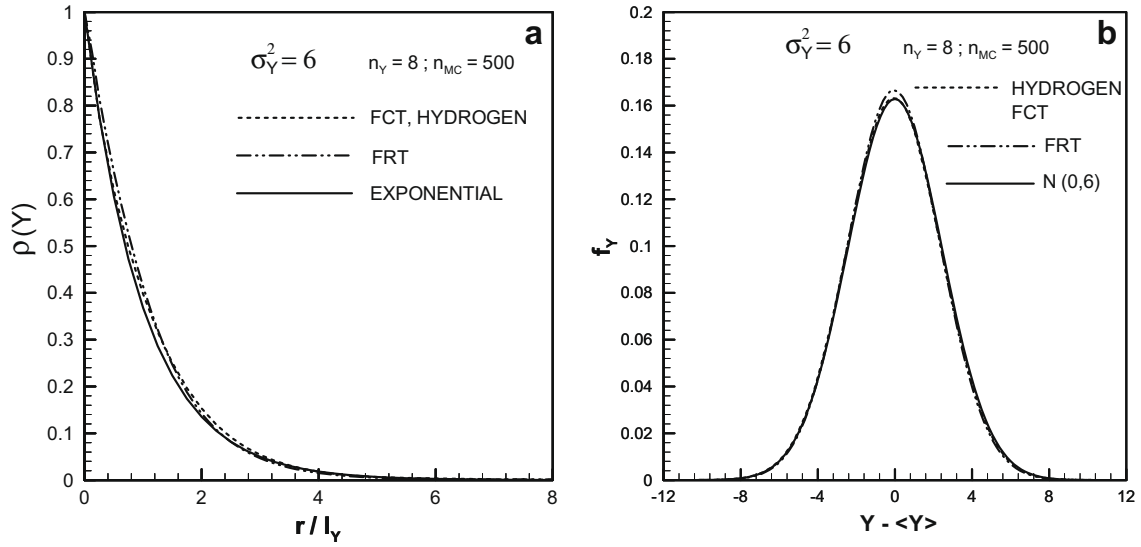

Fig. 6. Log-conductivity ensemble statistics: (a) autocorrelation of the log-conductivity field and (b) log-conductivity pdf obtained by HYDRO_GEN, FCT and FRT using $n_Y = 8$, 500 Monte-Carlo realizations, exponential covariance and $\sigma_Y^2 = 6$.

has its own particular resolution which means that log-conductivity and head do not need the same grid as it is common with all conventional numerical FE and FD methods. Each variable as well as velocity is obtained as a continuous function in form of linear combination of *Fup* basis functions which is essential for the particle tracking algorithm to be proposed in this work.

We consider steady groundwater flow (1) and (2) in two-dimensions characterized by constant porosity and heterogeneity represented by a spatially varying log-conductivity field through the (3) and (4) or its AFCM formulation (30)–(32). Eq. (3) and its AFCM counterpart (32) present an advection–dispersion equation (ADE). Log-conductivity variability and heterogeneity is represented by its derivatives, which act as an advective term in sense of the classic transport ADE. For small heterogeneity, the parabolic problem (3) and (4) converges to an elliptic one or a simple Laplace equation, but high heterogeneity transforms a parabolic problem (3) and (4) to an "advection-dominated" or a quasi-hyperbolic problem. Numerical implementation of (3) and (4) can be done in many ways. AFCM uses a strong formulation and directly solves the flow problem (3) and (4) by a collocation algorithm in such way that head solution is represented by a linear combination of *Fup* basis functions. Since AFCM uses collocation algorithm, mathematical model (3) and (4) is transformed to the non-symmetric and sparse system of linear algebraic equations (30)–(32). It is opposite to the conventional FE algorithms, for instance, where flow formulation (1) and (2) is presented by, through weak integral Galerkin formulation, elliptic problem and a symmetric, sparse system of linear algebraic equations. Salandin and Fiorotto [57] commented that spectral methods outperform FE solution mainly due to the log-conductivity continuity, but weakness of the classic spectral approach is neglecting the cutoff frequencies. AFCM presents also a spectral approach, but due to localized *Fup* basis functions, all log-conductivity and head frequencies are resolved. Consequence is solving of the non-symmetric linear system, instead of a symmetric one. Non-symmetric part of (3) is the advective term or log-conductivity derivatives. Higher $\ln K$ variance implies higher degree of heterogeneity and increasingly stronger non-symmetric linear systems.

An efficient GMRES solver [55] based on Krylov subspaces methods are implemented in this work using a multiplicative Schwarz preconditioner [56]. Briefly, the domain is divided into a number of mutually overlapping longitudinal blocks or subdomains. This preconditioner is essentially the same as the block Gauss–Seidel preconditioner and every block (submatrix) is factorized by a direct band solver; coefficients from other blocks (submatrices) are used from the last possible iteration and replaced to the right side. This preconditioner is very powerful because all non-zero matrix coefficients are included in the partial factorization.

Numerical experiments show that optimal results can be obtained for block width greater or equal to two integral scales with overlapping greater or equal to one integral scale, with the Krylov subspace equal to 100. Fig. 7 shows the convergence setup for one chosen realization (Fig. 5). Log-conductivity is approximated at level 2 or 8 points per integral scale ($n_Y = 8$), while head is solved at level 3 which has 16 points per integral scale ($n_h = 16$) or 528,905 unknowns and at level 4 which has 32 points per integral scale ($n_h = 32$) or 2,106,377 unknowns. Fig. 7 confirms that GMRES solver is very accurate due to small obtained residual norm and relatively fast due to a reasonable number of iterations. CPU time for this typical realization is around 10 min for level 3 ($n_h = 16$) and 1.5 h for level 4 ($n_h = 32$). Differences between realizations for

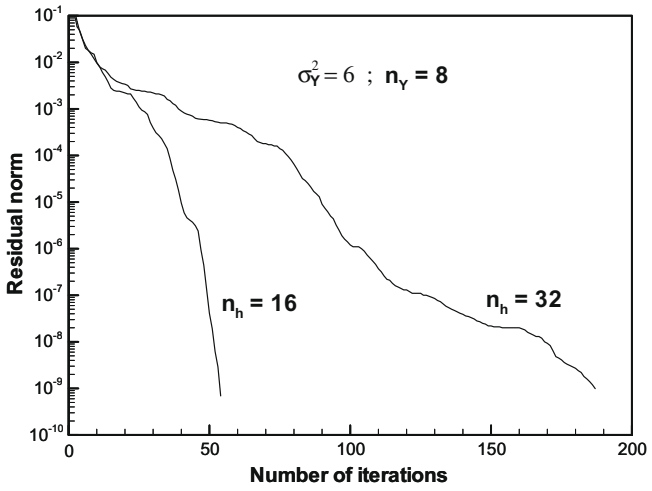

Fig. 7. GMRES convergence results for one chosen realization from Fig. 5 with exponential covariance, $n_Y = 8$, $\sigma_Y^2 = 6$ and two different head resolution levels: $n_h = 16$ and $n_h = 32$.

the same variance are relatively small and fluctuate around 10% of the average CPU time. MC simulations in this paper are done in cluster Lenggren on KTH-NADA Parallel Computer Centre (PDC, on dual-core Intel Xeon processors with 2.33 GHz and 8 GB RAM). Note that multiplicative Schwarz preconditioner requires at highest level 4 ($n_h = 32$) around 7 GB RAM for partial factorization. Further improvement should be the design of a parallel GMRES solver in order to use the full capacity of a cluster.

The flow equation acts as a filter of the heterogeneous log-conductivity field and head boundary conditions to the relatively smooth head solution. Consequently, input (log-conductivity) and output (head) have different statistical properties and generally do not require the same resolution. Therefore, due to its simplicity and generality, AFCM considers each variable as a separate function, enabling different resolutions for the input and output.

4.3. Hydraulic head and velocity solutions

Fig. 8 presents a multi-resolution head and streamline solution at the highest level 4 ($n_h = 32$) for different resolutions of the log-conductivity field ($n_Y = 4$–32; one chosen realization from Fig. 5). Although there are small differences between different log-conductivity resolutions, they cause small head differences, but larger streamline or velocity differences. Generally, flow or streamline patterns are similar for all log-conductivity resolutions, characterized by preferential flow channels [45], but shape, position and numbers of channels are slightly different. Different position of preferential flow channels implies traveling of one portion of the flow through different high-connected conductivity zones. Crucial question is how these log-conductivity differences influence flow and travel time statistics, as well as which log-conductivity resolution ensures accurate MC statistics (see Sections 5 and 6). Moreover, flow in low and mildly heterogeneous formations is relatively smooth and uniform and does not exhibit such complicated streamline patterns. Due to channeling, nonlinear effects appear to be dominant.

Finally, Fig. 8 presents streamline fields that are obtained from the AFCM continuous velocity approximation. This inherent AFCM property is a significant advantage in comparison to the conventional FE algorithms. Cordes and Kinzelbach [8] proposed a post-processor which creates a continuous velocity approximation from the ordinary FE head solution. Alternatively, a mixed FE formulation is required [46]. Moreover, continuous velocity approximation is necessary for accurate and reliable particle tracking that will be explored in the sequel. Relative accuracy of the velocity is lower, around one order of magnitude compared to the head accuracy, due to strong *Fup* correlation with the polynomial type of approximation. Note that FCT or FRT can also be used as a post-processor which yields a continuous velocity approximation from the classic FE head solutions (being thus a possible alternative to the *Cordes* and *Kinzelbach* approach).

Fig. 9 shows two head and streamline solutions at levels 3 and 4 ($n_h = 16$–32) for log-conductivity field at level 2 ($n_Y = 8$) and the realization from Fig. 5. Differences between two levels are relatively small for head, but it causes larger differences for streamline patterns. Head difference between third and fourth levels presents head contribution of the fourth level and it is in the dimensionless form $\Delta h/\Delta H < 0.029$ over the entire domain. This would imply that

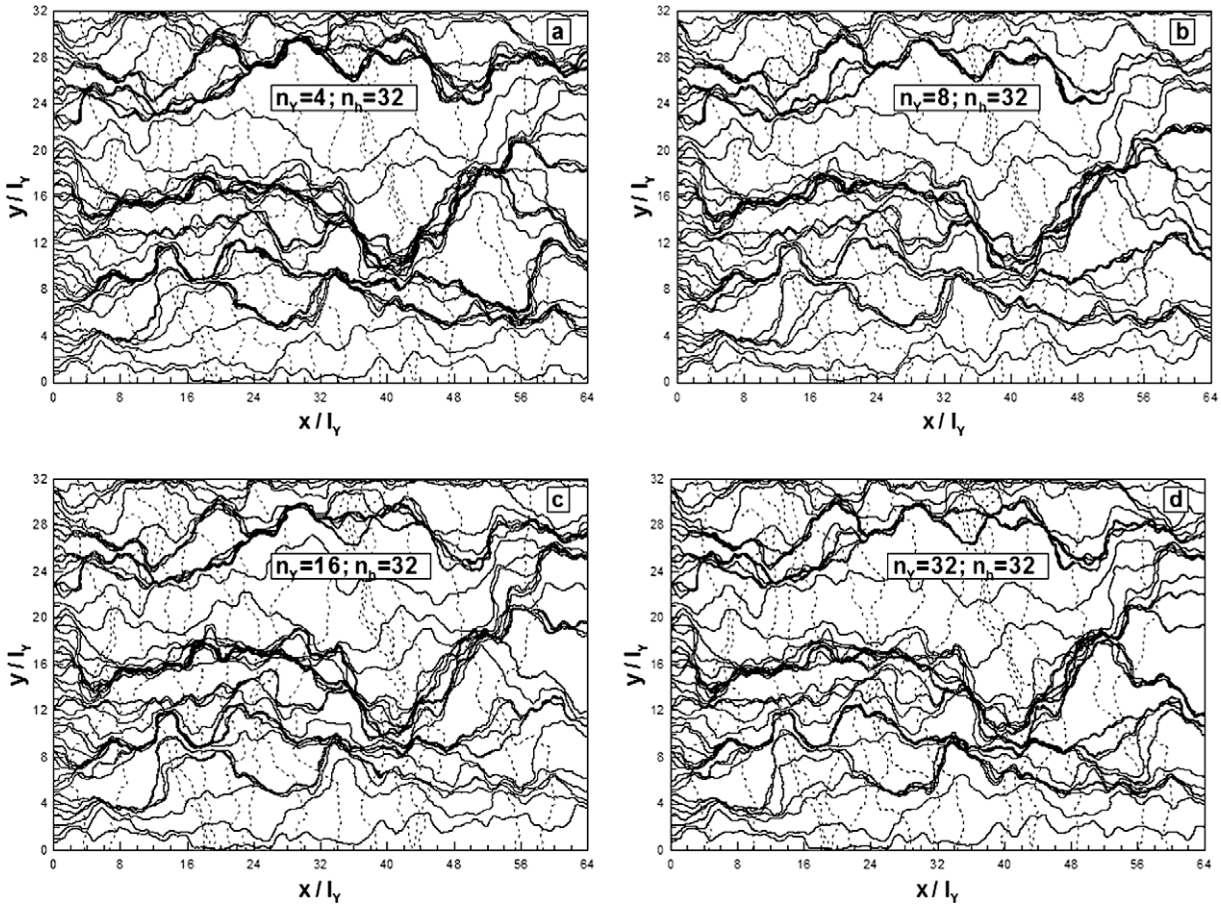

Fig. 8. Multi-resolution Fup approximation of the head and streamline field (one chosen realization from Fig. 5) with exponential covariance and $\sigma_Y^2 = 6$ for different resolution levels of the generated conductivity field ($n_h = 32$ and domain is $64l_Y * 32l_Y$): (a) $n_Y = 4$; $j = 1$, (b) $n_Y = 8$; $j = 2$, (c) $n_Y = 16$; $j = 3$ and (d) $n_Y = 32$; $j = 4$.

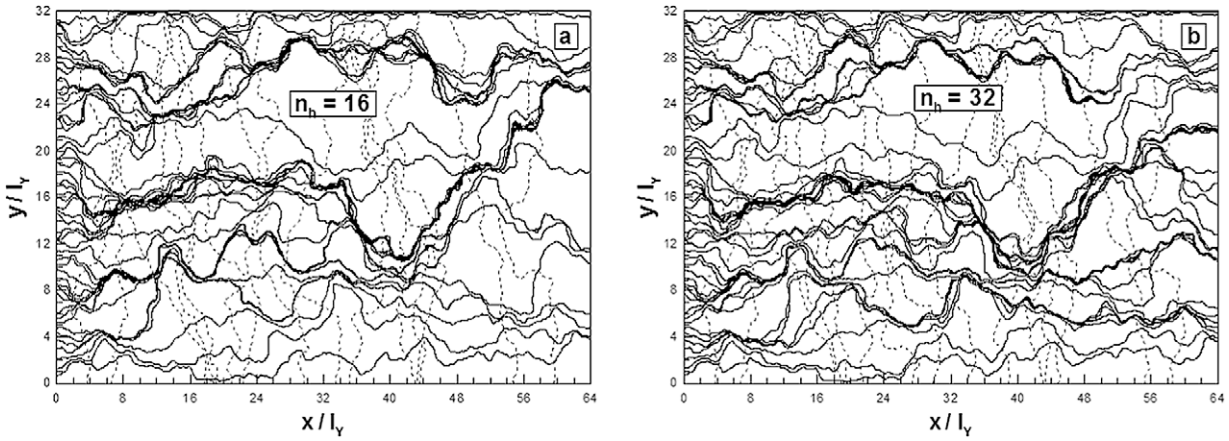

Fig. 9. Multi-resolution Fup approximation of the head and streamline field (one chosen realization from Fig. 5) with exponential covariance and $\sigma_Y^2 = 6$ for different resolution levels of the head field ($n_Y = 8$ and domain is $64l_Y * 32l_Y$): (a) $n_h = 16$; $j = 3$ and (b) $n_h = 32$; $j = 4$.

the computed head solution ($n_h = 32$; Fig. 9b) and "exact" unknown solution for this log-conductivity resolution should differ less than $\Delta h/\Delta H = 0.029$. Usually, this difference is overestimated which means that level 3 ($n_h = 16$) and especially level 4 ($n_h = 32$) are already quite accurate.

5. Accuracy and convergence of the flow solver

5.1. Flow-related Peclet number and other adaptive criteria

Head solution requires very fine resolution in order to satisfy detailed heterogeneity variations and accurately solve differential flow equation (3). It is constrained by an anisotropic *flow Peclet number* (in analogy to the transport Peclet number for advection–dispersion) defined by:

$$Pe_x = \frac{\partial Y}{\partial x} I_Y; \quad Pe_y = \frac{\partial Y}{\partial y} I_Y \tag{40}$$

On the other side, AFCM flow implementation (30)–(32) is constrained by an anisotropic *grid flow Peclet number* defined by:

$$Pe_{gx} = \frac{\partial Y}{\partial x}\frac{I_Y}{n_h} \leqslant 2; \quad Pe_{gy} = \frac{\partial Y}{\partial y}\frac{I_Y}{n_h} \leqslant 2 \tag{41}$$

Grid flow Peclet number directly describes influence of the heterogeneity variations. AFCM must decrease this criterion in order to obtain a head solution without a significant amount of numerical dispersion and/or oscillations. It is analogous with the classic transport Peclet number and numerical analysis of the advection-dominated problem with very small longitudinal and transverse dispersivities. In effect, we are considering the flow problem (3) as an advection–dispersion process with a strongly variable advective term (log-conductivity derivatives) and constant unit dispersion.

A minimum resolution requirement can be obtained from Eq. (41) at each level as:

$$\Delta x_j \leqslant \frac{2}{\partial Y/\partial x}; \quad \Delta y_j \leqslant \frac{2}{\partial Y/\partial y} \tag{42}$$

Furthermore, AFCM satisfies mass balance global criterion and head local criterion, which ensures global mass conservation and direct estimation of the solution accuracy, respectively. We consider maximum mass balance error (%) between any two vertical control planes over the entire domain, which is a more rigorous criterion than the common mass balance error between global inflow and outflow. Numerical experiments show that every next level yields head correction which is greater than contribution from all other higher levels, implying that the head correction criterion is a direct measure of the AFCM accuracy.

5.2. Accuracy

AFCM accuracy is defined by two local criteria, flow Peclet number and head correction, and mass balance global criterion. Fig. 10 shows mean values of flow Peclet number (Eq. (40)) for different log-conductivity resolutions and variances over 500 MC realizations. Fig. 10a presents absolute average flow Peclet number over the entire domain, while Fig. 10b presents maximum absolute flow Peclet number as:

$$L_2(Pe) = \max_{x,y\in D}(|Pe_x(x,y)|, |Pe_y(x,y)|) \tag{43}$$

Since flow Peclet number depends only on log-conductivity derivatives and heterogeneity, it increases for higher log-conductivity resolution and variance, which implies more involved heterogeneity variations. Average Peclet number is the same in each realization, while maximum Peclet number fluctuate around 10% of the mean value for each σ_Y^2; typically, maximum Peclet number is 5–10 times higher than the average value.

We can directly calculate grid flow Peclet number from Fig. 10 and Eq. (41) dividing the flow Peclet number by n_h. If the grid flow Peclet number is less than 2 over the entire domain, numerical experiments show that the obtained solution is quite accurate. Moreover, if this criterion is greater than 2 only locally in some subdomains, it is also possible to get acceptable accuracy. Fig. 10b shows two dashed horizontal lines which represent flow grid Peclet criterion (Eq. (41)) for $n_h = 16$ and $n_h = 32$, respectively. For the highest resolution of heterogeneity ($n_Y = 32$), AFCM requires head resolution more than our temporal computational limit ($n_h = 32$ or 2.1×10^6 unknowns) for acceptable solution in cases $\sigma_Y^2 > 2$ in order to satisfy criterion (42). For lower heterogeneity resolution ($n_Y = 16$), maximum head resolution ($n_h = 32$) enables acceptable results for σ_Y^2 up to 4. For heterogeneity resolution ($n_Y = 8$), maximum head resolution ($n_h = 32$) enables quite accurate results for all σ_Y^2, while lower head resolution ($n_h = 16$) yields acceptable results for σ_Y^2 up to 4. For heterogeneity resolution ($n_Y = 4$), head resolution ($n_h = 16$) enables quite accurate results for almost all σ_Y^2. Note that Gaussian covariance yields considerably smaller Peclet numbers as it is shown for heterogeneity resolution ($n_Y = 8$) and head resolution ($n_h = 16$) (Fig. 10, [61]).

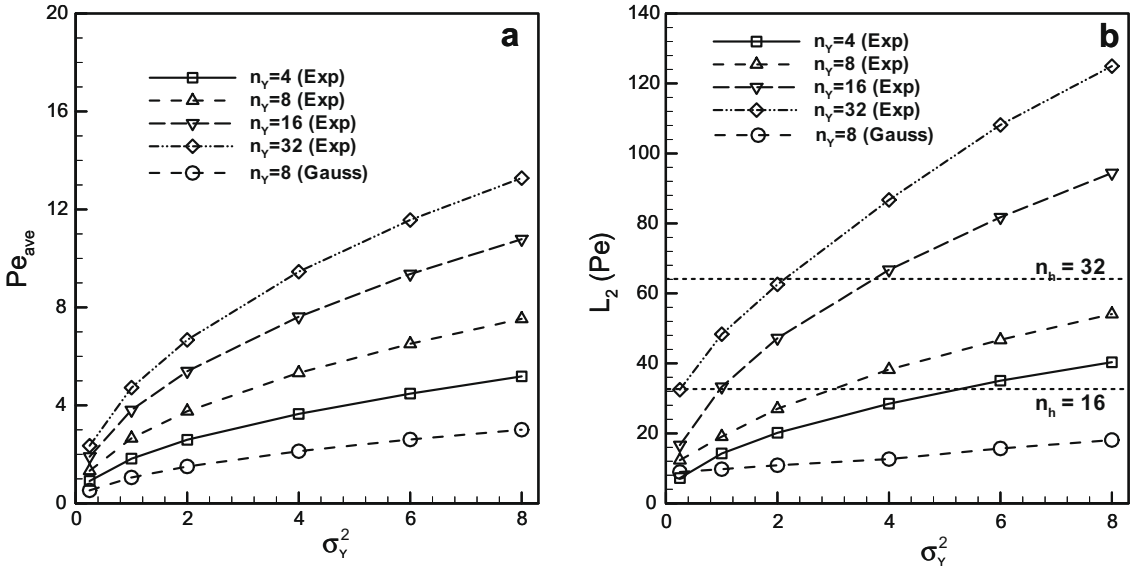

Fig. 10. Dependence of the log-conductivity variance and mean Peclet number (Eq. (40)) for different resolution levels of the generated conductivity field (500 Monte-Carlo realizations and domain is $64l_Y * 32l_Y$): (a) average absolute Peclet number, (b) maximum absolute Peclet number.

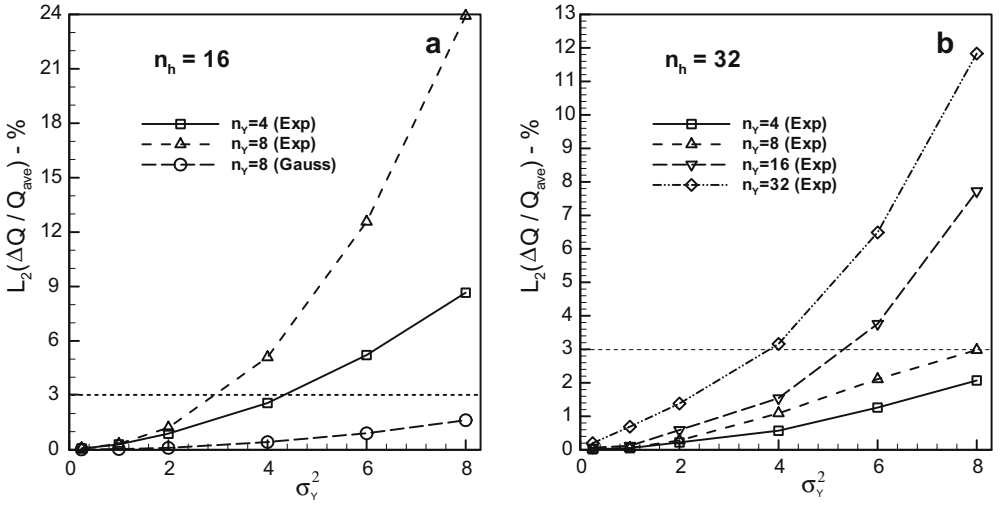

Fig. 11. Dependence of the log-conductivity variance and mean maximum relative difference of the flow discharge between different vertical cross-sections (500 Monte-Carlo realizations and domain is $64l_Y * 32l_Y$): (a) $n_h = 16$ and (b) $n_h = 32$.

Similar considerations are applicable to Fig. 11 for maximum relative mass balance error (%) between any two vertical control planes divided by average flow rate over the entire domain with: (a) lower head resolution ($n_h = 16$) and (b) maximum head resolution ($n_h = 32$). Fig. 11 presents mean values over 500 MC realizations and shows a dashed horizontal line for mass balance error of 3% which appears as upper limit for accurate and reliable flow and travel time statistics as will be shown in the sequel. Generally, for a mild heterogeneity (σ_Y^2 up to 2), head solution is quite accurate with a mass balance error less than 3% for all presented head and log-conductivity resolutions. However, for high heterogeneity ($\sigma_Y^2 > 3$) mass balance error tends to increase considerably, especially for the highest log-conductivity resolution ($n_Y = 32$). Lower head resolution ($n_h = 16$) gives quite accurate results only for $n_Y = 4$ and σ_Y^2 up to 4 and for $n_Y = 8$ and σ_Y^2 up to 2 (Fig. 11a). Maximum head resolution ($n_h = 32$) enables acceptable results for heterogeneity resolution ($n_Y = 16$) and σ_Y^2 up to 4, while it enables accurate results for lower heterogeneity resolutions ($n_Y = 4$–8) and all σ_Y^2 with mass balance error less than 3% (Fig. 11b). Once again, Gaussian covariance with $n_Y = 8$ and $n_h = 16$ gives very accurate flow results.

Fig. 12 shows mean values for head correction criterion over 500 MC realizations; this figure is closely related to Fig. 9. We used two head resolution levels ($n_h = 16$–32) and log-conductivity resolutions ($n_Y = 4$–8). Therefore, head correction solution is obtained at maximum head resolution ($n_h = 32$) because AFCM on that resolution finds only difference or residual between head solution at $n_h = 16$ and $n_h = 32$. For $n_Y = 8$, head correction in the dimensionless form is less than 0.06 or 6% of total head drop ΔH for all $\ln K$ variances, which is an acceptable head solution. Furthermore, for $n_Y = 4$, head correction is less than 2% of total head drop for all $\ln K$ variances, similar to the results for a Gaussian covariance with

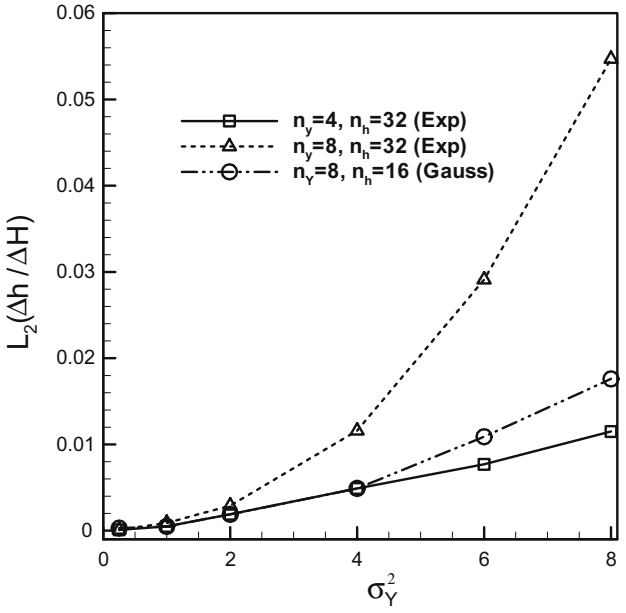

Fig. 12. Dependence of the log-conductivity resolution and mean head correction criterion (500 Monte-Carlo realizations and domain is $64l_Y * 32l_Y$) for exponential ($n_Y = 4$ and $n_Y = 8$; $n_h = 32$) and Gaussian ($n_Y = 8$; $n_h = 16$) covariance.

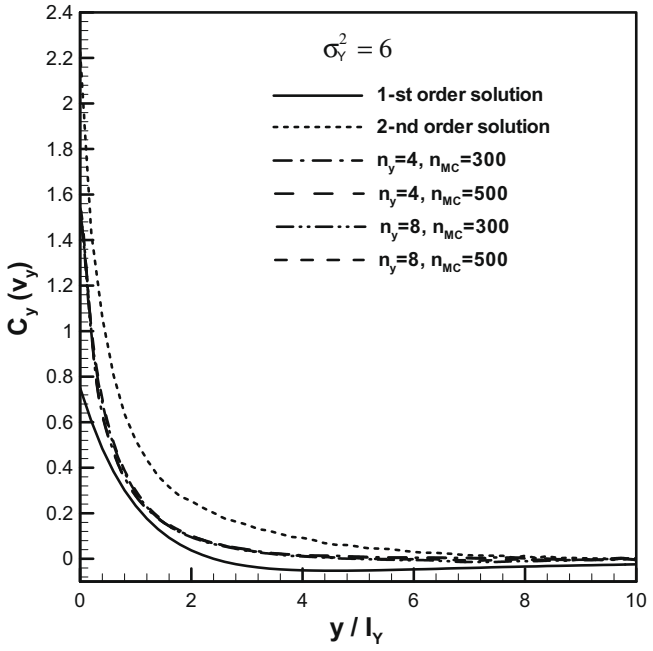

Fig. 14. Dependence of the log-conductivity resolution and number of Monte-Carlo realizations on transverse velocity covariance for highly heterogeneity case with exponential covariance and $\sigma_Y^2 = 6$.

$n_Y = 8$ and $n_h = 16$. Note that this criterion usually overestimates real head errors that are proved with small mass balance errors for respective resolutions.

5.3. Convergence

Convergence analysis focuses on the influence of the log-conductivity resolution and number of MC realizations on ensemble statistics. Velocity covariance requires larger resolution level only for lags smaller than the grid size, i.e. for variance calculation [58]. Fig. 13 presents influence of the log-conductivity resolution on the longitudinal and transverse Eulerian velocity variance. Exponential log-conductivity covariance theoretically requires head resolution which tends to zero in order to capture all heterogeneity variations. Practically, results show that resolution $n_Y = 8$ ensures accurate velocity variances for all σ_Y^2 due to reasonable difference between velocity variances for cases $n_Y = 4$ and $n_Y = 8$. Furthermore, for $\sigma_Y^2 > 4$, $n_Y = 16$ and $n_h = 32$ values of velocity variances decrease due to influence of the numerical dispersion and mass balance error higher than 3%. Evidently, AFCM requires head resolution more than our temporal computational limit ($n_h = 32$ or 2.1×10^6 unknowns) because in these cases numerical errors smooth the velocity field whereby physically more logical variances are obtained with lower heterogeneity resolution.

Fig. 14 presents transverse velocity covariance with $\sigma_Y^2 = 6$, $n_h = 32$ and four considered cases: (a) $n_Y = 4$, $n_{MC} = 300$, (b) $n_Y = 4$, $n_{MC} = 500$, (c) $n_Y = 8$, $n_{MC} = 300$ and (d) $n_Y = 8$, $n_{MC} = 500$.

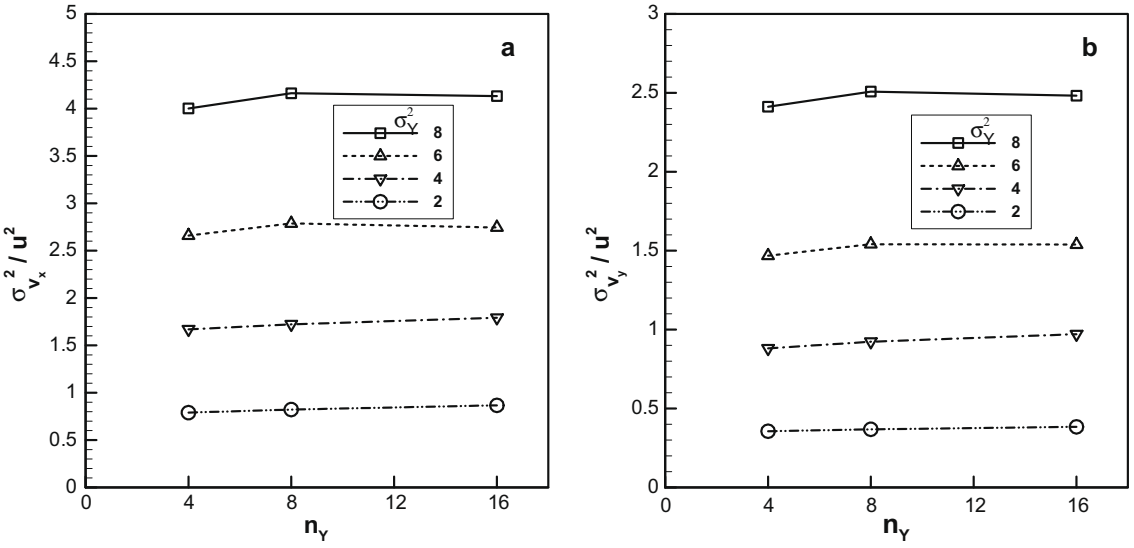

Fig. 13. Dependence of the log-conductivity resolution and Eulerian velocity variance (500 Monte-Carlo realizations, $n_h = 32$ and domain is $64l_Y * 32l_Y$): (a) longitudinal velocity variance and (b) transverse velocity variance.

Velocity variance as well as the covariance is bounded by first- and second-order theory as lower and upper bound, respectively. Variance is closer to the second-order results [32], while ensemble results of Salandin and Fiorotto [58] for $\sigma_Y^2 \leqslant 4$ are relatively accurate despite some inaccuracies in each realization. We can conclude that both analytic solutions poorly represent transverse velocity covariance for $\sigma_Y^2 = 6$. Differences between cases *c* and *d* as well as *b* and *d* are very small and practically negligible, except partly at the origin. It confirms that 500 MC realizations are sufficient in order to eliminate statistical error. In particular, relative differences between transverse (as well as longitudinal) velocity covariance obtained from 300 and 500 MC realizations are less than 3%. Since it is well known that MC statistical error decreases very slowly and proportionally with $n_{MC}^{-0.5}$, we conclude that 500 MC realizations are sufficient in order to keep statistical error comparable to the other errors which arise from the MC procedure. Therefore, overall results of this subsection show that resolutions $n_Y = 8$ and $n_h = 32$ as well as 500 MC realizations ensure accurate velocity ensemble statistics in highly heterogeneous porous media with $\sigma_Y^2 \leqslant 8$.

6. Advective transport

Here, we focus on advective transport and compute transverse displacement and travel time for an unlimited number of advecting particles through the heterogeneous domain (Eq. (5)). Transport analysis is based on the approach of Cvetković et al. [10] who considered Langrangian variables as spatial fields. For current illustration, we choose the in flux injection mode, contrary to Cvetković et al. [9] who considered uniform (resident) injection mode [15].

6.1. Particle tracking algorithm

Application of the particle tracking technique requires only knowledge of the velocity field (Eq. (5)). However, in highly heterogeneous media, the spatial flow variation is large and characterized by preferential flow channels and barriers. Therefore, traditional particle methods can fail due to following three sources of errors: discontinuous and grid based velocity approximation, inaccurate numerical integration and insufficient number of particles.

As we explained above, AFCM naturally produces continuous velocity fields, while conventional methods require special postprocessor [8] or formulation [46]. Moreover, as reported by LaBolle et al. [43], velocity values are always given in the finite element nodes or finite difference cells, while velocity interpolation (usually linear, bilinear or even constant) is done inside each element or cell according to these velocity values. Velocity approximation is thereby grid dependent on discrete calculated values and particle tracking algorithm is constrained by classic Courant criterion that particles may not cross more than half of the cell or element width in each direction. In comparison, AFCM provides continuous velocity fields in analytic form of linear combination of the *Fup* basis functions. This implies that velocity approximation in each point is defined with the same accuracy as the grid independent field where the advective step is *not* constrained by the Courant criterion.

Here, we use Runge–Kutta–Verner explicit temporal numerical integration scheme of the fifth and sixth order with eight stages in Eq. (5) [66]. Nodes, weights and linking coefficients are usually presented in the Butcher tableau [66]. Adaptive time step is accepted if difference between solutions of the fifth and sixth order is less than the prescribed threshold (local integration error). Runge–Kutta–Verner scheme enable greater time steps than standard lower schemes. We track each particle independently using as small as possible time steps in order to cross an arbitrary CP. If we require some intermediate values of the displacement or travel time, sixth order polynomial interpolation from the calculated values should be performed. Importantly, the same sixth order of interpolation and Runge–Kutta–Verner scheme guarantees that calculated values at all locations are obtained within the same accuracy.

Finally, we will examine how many particles are needed in order to obtain accurate MC ensemble statistics. Using the ergodic hypothesis, our objective is to use as larger number of particles as possible and therefore decrease the number of realizations in order to stabilize MC higher-order moments and pdf's. Bellin et al. [4] found that 1500 MC realizations are needed for displacement variance and only one particle in the each realization for mild $\ln K$ variance up to 1.6. However, Salandin and Fiorotto [58] found that only 500 MC realizations are sufficient for Langrangian velocity covariance, but they used up to 20,000 particles in the each realization for high $\ln K$ variance up to 4. We present here a new particle tracking strategy which yields a solution of travel time and transverse displacement for all particles. If we consider a steady and continuous velocity field, transverse displacement and travel time defined on streamlines are continuous, and there is continuity between any two close adjacent streamlines. If we know all streamlines or infinite number of particles, it is possible to describe transverse displacement or travel time field as continuous function in each realization.

At the zeroth level, we choose a relatively small number of equally 'in flux' distributed particles and find displacement and travel time for each particle from the source area to the arbitrary control plane. FRT gives zeroth level continuous approximation for displacement and travel time based on calculated discrete particle values. In the first level, two times more particles are tracked and FRT first level continuous approximation is obtained. Then, residual between the zero and first level is checked. In the next level, FRT will add particles only in the zones where residual is greater than the prescribed threshold. Up to the final level, FRT will approximate displacement and travel time to the desired accuracy and determine how many particles are needed to obtain such solution. In this manner, FRT will approximately calculate all particles and variables defined on them in the form of an analytic continuous function. However, FRT finds only a minimum number of particles in order to describe transport variables for all particles. Consequently, there is some difference between FRT and exact solution, but it is less than the prescribed threshold which guarantees obtaining transport variables with desired accuracy.

Transfer between the discrete and continuous forms is one of the most important properties of the presented approach. If the FRT reaches desired accuracy in each realization, this means that ensemble averaging cannot introduce additional errors. In the next subsection we will present 1-D and 2-D transverse displacement and travel time multi-resolution approximation. Note that extending this algorithm to 3-D flow fields and/or unsteady velocity fields is straightforward.

6.2. Transverse displacement and travel time fields

Using the particle tracking method explained above, a multi-resolution approximation of the transverse displacement $\eta(y_0; x)$ and travel time $\tau(y_0; x)$ is presented in Fig. 15 for arbitrary control plane at distance $x/I_Y = 52$ if source area is located at distance $x/I_Y = 12$, while the vertical axis y_0 represents coordinate of a particle within the source area.

Fig. 15 illustrates a high variation of both variables for the single realization in Fig. 5. Each dominant flow channel occupies some significant portion of the vertical axis. So, lower velocity zones

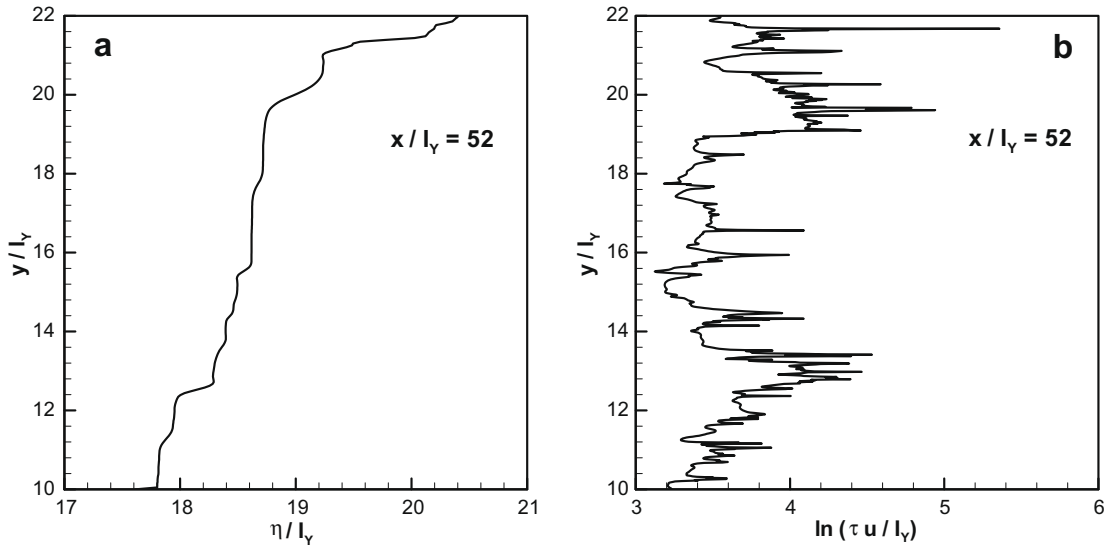

Fig. 15. 1-D transverse displacement (a) and travel time (b) distribution for one chosen realization from Fig. 5 with exponential covariance and $\sigma_Y^2 = 6$ ($n_Y = 8$, $n_h = 32$, $x/I_Y = 52$).

occupy only small portion of the vertical axis. Transverse displacement (Fig. 15a) has similar value for an entire channel, but sharp changes or fronts are recorded in the lower velocity zones, which separate dominant flow channels.

The travel time distribution (Fig. 15b) is also influenced by position of the dominant flow channels, but mainly with 'temporal history' of each streamline. Higher level of heterogeneity causes more complex 'temporal history' because some streamlines or trajectories belong to the one dominant channel, but after some time transfer to another channel or to low permeable zones and vice versa. We can conclude that the travel time field contains a lot of information about heterogeneity and velocity fields exposing a complex structure.

Figs. 16 and 17 present 2-D transverse displacement and travel time distributions from the chosen realization (Fig. 5), respectively. Solutions are obtained in the transformed domain such that vertical and horizontal lines represent control planes and streamlines, respectively. Vertical axis has the same meaning as in Fig. 15. Figs. 16 and 17 represent solutions for all control planes and streamlines in the inner computational domain in order to avoid influence of the flow boundary conditions. Fig. 16a shows transverse displacement field structure. In the vertical direction or in each *CP*, transverse displacement has the monotonic slope because advective transport streamlines do not cross each other. In the horizontal direction or for each streamline, transverse displacement fluctuates around the mean position, and the function is more complicated. Note that values of the presented transverse displacement field $\eta(y_0; x)$ in Fig. 16a must be decreased by initial source position $\eta(y_0; x_0)$ in order to obtain transverse displacement field according to Eq. (6).

Travel time has the monotonic slope in the horizontal direction because more distant CP requires longer travel time, while the function is more complex in the other direction due to abrupt changes between different particles within the CP (Fig. 17a). Both fields show a complex structure, which is mainly caused by high heterogeneity. This unique presentation clearly shows significant difference between relatively close control planes and/or streamlines. Note that we consider here function $\tau(x)$ for each particle. Its inversion leads to classic displacement function $X'(t)$, required for calculation of the macrodispersion tensor. Both fields are obtained with desired accuracy, which is defined by the prescribed threshold. Relative accuracy of less than 0.1% satisfies all our practical requirements.

Figs. 16b and 17b present adaptive grid or distribution of collocation points for transverse displacement and travel time fields, respectively. Adaptive grid shows not only the minimum collocation points needed for describing both fields with desired accuracy, but also all spatial scales which represent solutions. Due to different behavior, adaptive grids of both variables are different. This implies that the presented adaptive procedure "finds" a particular grid for each variable resolving only important spatial scales. Higher levels or finer scales and resolutions are required in zones where fields exhibit sharp changes due to fluctuating streamlines, transfers between dominant channels, interchanging of the lower and higher velocity zones and maybe some other approximation reasons. Transverse displacement requires less streamlines, but more polynomial interpolation within the streamline. Travel time requires more streamlines and collocation points due to more complex structure. For this realization ($\sigma_Y^2 = 6$) around 4000 particles and 200,000 collocation points were required to obtain such accurate solutions. Typical realization can fluctuate only 10% around average quantities. Smaller variances require a considerably lower number of particles due to absence of nonlinear effects.

6.3. Convergence

Accuracy is defined by the prescribed threshold in each realization. Only convergence aspects remain to be analyzed in this subsection. As in the flow analysis described earlier, influence of the log-conductivity resolution and number of MC realizations is of interest. Fig. 18a and b presents pdf's of the transverse displacement and travel time for four cases with $\sigma_Y^2 = 6$: (a) $n_Y = 4$, $n_{MC} = 300$, (b) $n_Y = 4$, $n_{MC} = 500$, (c) $n_Y = 8$, $n_{MC} = 300$ and (d) $n_Y = 8$, $n_{MC} = 500$. Differences between cases *c* and *d*, and also *b* and *d* are relatively small, especially for travel time. Transverse displacement pdf requires more realizations due to small remaining statistical oscillations, which do not change global accuracy of the pdf. Therefore, results show that the resolution $n_Y = 8$, relative accuracy less than 0.1% in each realization and 500 MC realizations ensure accurate pdf's of the transverse displacement and travel time ensemble statistics.

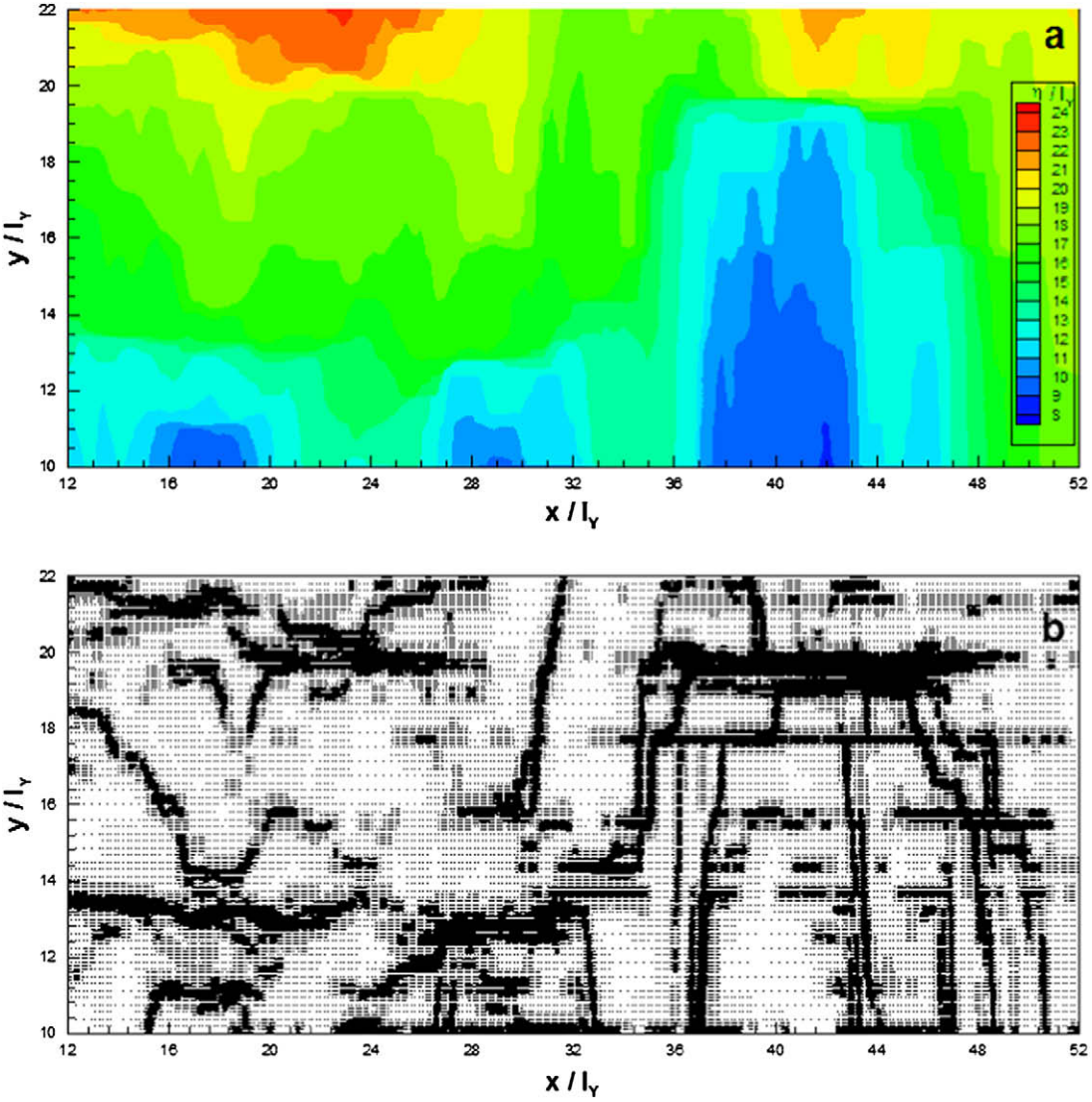

Fig. 16. Transverse displacement field (a) and corresponding adaptive grid (b) from one chosen realization (Fig. 5) in the inner computational domain with exponential covariance and $\sigma_Y^2 = 6$ ($n_Y = 8$, $n_h = 32$, threshold is 0.02).

7. Discussion

The proposed Adaptive Fup Monte-Carlo Method (AFMCM) represents a general framework for flow and transport in highly heterogeneous porous media which uses a novel form of the adaptive collocation method AFCM for the differential flow equation and the Fup transformations for log-conductivity and transport approximations, respectively (Fig. 2). This methodology enables a multi-resolution of different spatial and temporal scales for all flow and transport variables. The main idea behind this approach is finding separately the minimum number of collocation points and resolution levels to describe each flow and transport variable with desired accuracy on a particular adaptive grid. Therefore, adaptive and multi-scale nature of the methodology enables not only computational efficiency and accuracy, but describes subsurface processes closely related to their understood physical interpretation.

AFMCM combines the most desirable properties of existing numerical methods: (1) localized basis functions as in conventional FE, (2) application of strong formulation and simple procedure as in conventional FD, (3) accuracy and continuity of basic variables and their derivatives and usage of Fup transformations as in spectral methods, and (4) adaptive and efficient procedure with error estimation as in all modern numerical approaches.

Monte-Carlo methodology needs to describe and interconnect log-conductivity, flow and transport approximations. Crucial and the most demanding MC step is the flow solver which uses the log-conductivity field as input and yields the velocity field as output based on Eqs. (3) and (4). Representation of the log-conductivity field as well as its approximation used in any particular numerical procedure strongly affects the obtained velocity field. The main task for a flow solver is obtaining continuous velocity fields which enable accurate and efficient particle tracking and transport approximations, especially in highly heterogeneous porous media. Traditional FE methods with linear or bilinear head interpolations result in velocity discontinuities between elements with different conductivity. Continuous velocity field can be obtained by special flow post-processing [8,58] or with a mixed FE formulation [46] whereby velocities across element sides are constant and continuous. All these procedures require non-negligible additional computational resources and efforts.

Stream formulation inherently yields continuous velocity fields and streamlines for particle tracking, but they are difficult to implement for 3-D and/or transient problems with sink-sources

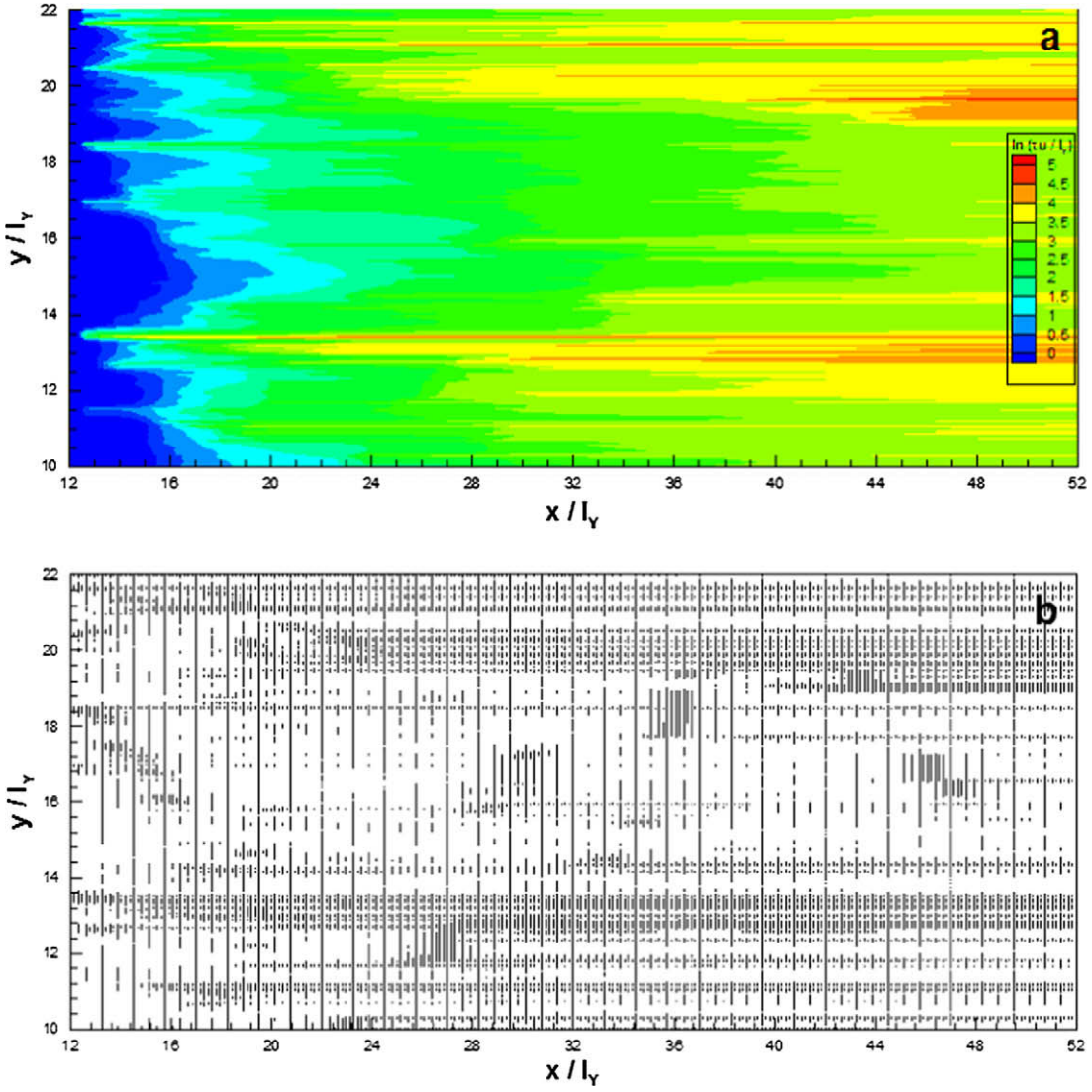

Fig. 17. Travel time field (a) and corresponding adaptive grid (b) from one chosen realization (Fig. 5) in the inner computational domain with exponential covariance and $\sigma_Y^2 = 6$ ($n_Y = 8$, $n_h = 32$, threshold is 0.001).

[6,22]. Contrary, block centered FD scheme (essentially close related to the finite volume formulation) where the head in the center of block are obtained by applying a mass balance over the edges of the block [17], gives continuous and constant velocities across block sides as in FE models without additional CPU efforts. These methods usually imply Pollock semi-analytic particle tracking procedure and exact derivation of travel time and displacement in each block or element [48]. Note that the Pollock procedure implies continuous velocity in each point in the sense of bilinear interpolation from the edge velocities.

By comparison, AFMCM uses continuous a log-conductivity field (FRT) and collocation algorithm for the flow approximation (AFCM). Disadvantage of this approach lies in the fact that an elliptic problem is transformed to the advection–dispersion problem and global mass conservation is violated due to the collocation nature of the algorithm. Therefore, for high heterogeneity our head solution requires higher resolution than log-conductivity in order to obtain an accurate solution and decrease the Peclet number (related to the log-conductivity variations) and mass balance error (Figs. 10–14). However, AFMCM yields continuous velocity fields with the same accuracy in each point which significantly outperforms (low-order) conventional mentioned methods. Furthermore, efficient particle tracking can use higher and more accurate time integration schemes along the streamlines and without additional effort include as many particles as are needed in order to accurately present travel time, transverse displacement and/or other transport variables. The drawback, as mentioned, is that accuracy, multi-resolution and other AFMCM properties require a relatively expensive flow solver.

On the other side, novel finite element and other multi-scale methods try to find fine scale velocity solution on coarse grid using the only most relevant fine scale information [20]. However, velocity error due to loss of particular fine scale information can play a key role for some important features of flow and transport in highly heterogeneous porous media such as early arrivals, travel time peaks and tailings, asymptotic dispersivity or higher-order moments. Unfortunately, it means that usually we need fine scale velocity field which require extensive CPU resources for extensions to 3-D flows for all aforementioned approaches. Since an extension of AFMCM to 3-D flow and transport problem is conceptually straightforward, the 3-D flow solution with the presented approach is still an open problem due to a large linear system of equations ($O(10^9$–$10^{11})$) which can outperform even existing parallel supercomputer capabilities [7,17,34]. Analysis of

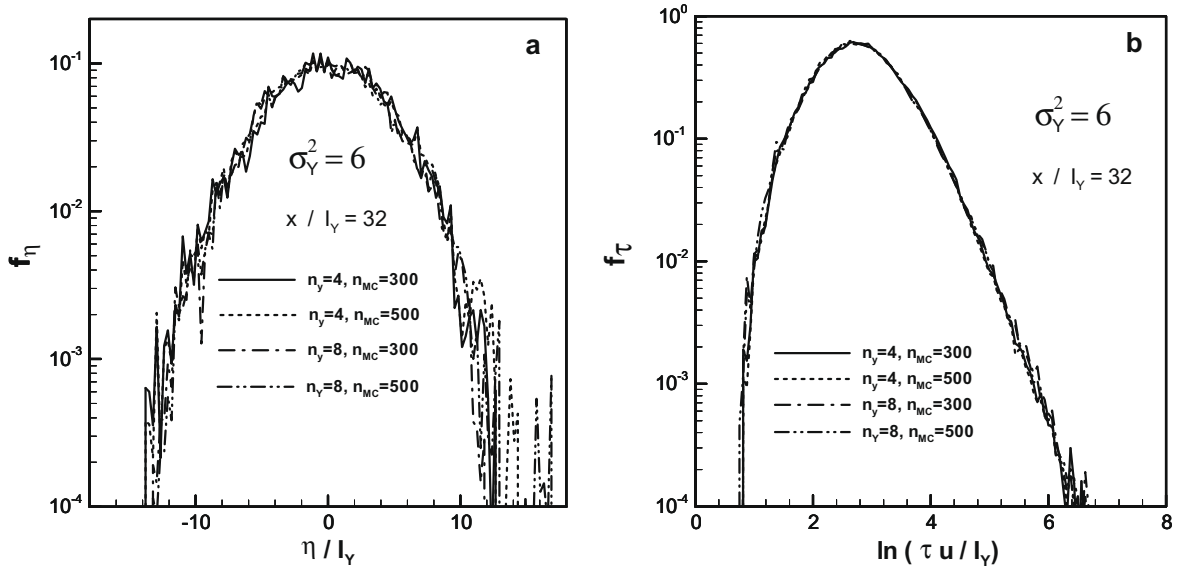

Fig. 18. Dependence of the log-conductivity resolution and number of Monte-Carlo realizations on pdf of the transverse displacement and travel time for highly heterogeneity case with exponential covariance, middle control plane and $\sigma_Y^2 = 6$.

multi-Gaussian heterogeneity fields with other correlation structures (such as Gaussian correlation, Figs. 10–12) or other non-Gaussian and fractal fields could yield more correlated structures and significantly smaller Peclet numbers (Fig. 10) and mass balance errors (Fig. 11). Therefore, AFMCM can describe more efficiently such fields using the adaptive multi-resolution grid, compared to the classic multi-Gaussian case with exponential correlation which has become the standard prototype statistical model for numerical and analytical studies. Alternative heterogeneity structures, for which AFMCM can be much more readily extended to 3-D flows, are relevant for applications and are the topic of our current research.

The main remaining numerical problem for mesh-free collocation methods with localized basis functions such as Fup (atomic), wavelets or splines is solving flow for irregular geometries. Although adaptive Fup approach essentially solves irregular geometry on higher levels by appropriate adaptive a priori criteria, there are still a number of implementation problems when satisfying all geometry requirements. It is worthwhile noting that work is currently in progress to extend the presented methodology to problems with irregular geometry.

Due to its adaptive properties, accuracy and convergence analysis using AFMCM enables direct estimation of the error in each step of the MC procedure. Accuracy is primarily defined by the particular prescribed threshold for each variable. Convergence analysis proved that resolutions of $n_Y = 8$ and $n_h = 32$, 500 MC realizations and around 4000 particles are sufficient for accurate ensemble statistics for all flow and transport variables in highly heterogeneous porous media with $\sigma_Y^2 \leqslant 8$. There were no accuracy and convergence analysis of the FE flow solution of Salandin and Fiorotto [58] who used ($n_Y = n_h = 8$) for σ_Y^2 up to 4 and FD solution of de Dreuzy et al. [17] with $n_Y = n_h = 10$ and σ_Y^2 up to 9. In sense of AFMCM accuracy, both studies have maximum grid flow Peclet number greater than four, while mass balance error is higher than 10% which is quite significant (Figs. 10 and 11). Their low-order conventional solutions exactly satisfy mass conservation, however local accuracy of the computed velocity fields which directly affects transport computations, has yet to be shown as satisfactory. Note that for σ_Y^2 up to 4 both Eulerian velocity variances (Fig. 13) are in a close agreement with their solutions, but de Dreuzy et al. [17] did not report results for $\sigma_Y^2 > 4$.

8. Conclusions

In this paper we presented a new Monte-Carlo methodology based on compactly supported *Fup* basis functions and a multi-resolution approach in order to obtain reliable flow and travel time statistics in highly heterogeneous porous media. We considered for illustration 2-D steady, linear and unidirectional flow of ($64I_Y * 32I_Y$) domain size with isotropic exponential correlation heterogeneity structure and $\ln K$ variance up to 8. Although MC method is appealing in its conceptual simplicity and generality, each MC step presents a potentially serious source of errors, especially for highly heterogeneous aquifers. In our study, strict accuracy and convergence analysis is performed in order to define which resolution level for all flow and transport variables is needed to obtain reliable flow and travel time statistics.

The main conclusions can be summarized as follows:

1. Log-conductivity field in each realization is presented by a continuous function (FCT or FRT) and a high resolution level ($n_Y = 4$–32 points per integral scale) reproducing very accurately prescribed covariance properties.
2. In each realization, head solution should satisfy grid flow Peclet number, head correction and mass balance criteria. Numerical experiments show that a high resolution level is needed to accurately solve the flow equation due to the large variability in hydraulic properties. If grid flow Peclet number is satisfied over the entire domain, other two criteria usually show acceptable accuracy.
3. Velocity is obtained as a continuous function and a mesh-free field with the same accuracy in each point of the domain, which enables the formulation of an accurate particle tracking algorithm and transport analysis.
4. Results indicate that resolutions $n_Y = 8$ and $n_h = 32$ yields very accurate flow solutions in each realization with relative mass balance error smaller than 3% and quite accurate velocity covariance. Furthermore, high $\ln K$ variance and heterogeneity requires finer head resolution levels than the chosen log-conductivity resolution level.
5. Transport analysis based on the proposed particle tracking algorithm that uses high order Runge–Kutta–Verner (8,5:6) numerical integration scheme and Fup Regularized Transform (FRT)

tracks particles very accurately with adaptive time step controlling the local integration error. Moreover, the algorithm can represent all particles and variables defined on them such as transverse displacement and travel time as continuous function in an analytical form of linear combinations of Fup basis functions with desired relative accuracy (0.1%) in each realization. Furthermore, resolution $n_Y = 8$ and around 4000 particles in each realization ensures an accurate pdf of the transverse displacement and travel time.

6. All required flow and transport variables require up to 500 Monte-Carlo realizations in order to stabilize fluctuations of the ensemble statistics in highly heterogeneous formations with $\sigma_Y^2 \leqslant 8$.

Development of the adaptive Fup multi-resolution approach opens new possibilities for future investigations of advective transport in heterogeneous porous media. We are particularly interested in analysis of higher moments of the solute flux, reactive transport in t–τ domain (multi-resolution solving of the sharp fronts of different chemical species), analysis of concentration fluctuations and influence of the local pore-scale dispersion. Finally, our main objective in the next step is to use AFMCM to perform 3-D analysis of the aforementioned problems.

Acknowledgements

The authors wish to thank PDC staff (Parallel Data Center at KTH-NADA in Stockholm, Sweden) for valuable help during this work and K.-C. Hsu for the second-order results of velocity statistics. Comments and criticisms from anonymous reviewers have led to improvements in this work.

Appendix A

Accuracy of the collocation algorithm on the uniform grid can be shown by a certain list of theorems [40]. Since presented adaptive strategy does not decrease accuracy with respect to the uniform grid due to neglecting collocation points which does not contribute to the solution (e.g. Fig. 4), then it is possible to adapt analysis of Kravchenko and Basarab [40] to the multi-resolution grid and prove at each level:

Theorem 1. *If $u(x) \in C^n$, then exist Fup coefficients (a_k^j) in Eq. (16) such that*

$$\|u(x) - u^j(x)\| \leqslant K_n \Delta x_j^{n-1} \omega_n(u; \Delta x_j) \tag{A1}$$

where K_n is a real number independent of Δx_j, but depends on n-Fup order, while $\omega_n(u; \Delta x_j)$ is the modulus of continuity:

$$\omega_n(u; \Delta x_j) = \max_{|x_0 - x_0^*| \leqslant \Delta x_j} \left| \frac{\partial^n}{\partial x^n} (u(x_0) - u(x_0^*)) \right| \tag{A2}$$

It means that generally Fup approximation depends on three factors: n-Fup order, Δx_j and derivative differences of the n-order inside the Δx_j.

Theorem 2. *If $u(x) \in C^{n+1}$ and a_k^j are Fup coefficients obtained by proposed collocation algorithm (FCT), then the approximation (16) satisfies the following relation:*

$$\|u(x) - u^j(x)\| \leqslant (1 + 2^n r^{-1}) \|u(x) - u_*^j(x)\| \tag{A3}$$

where $r = \varphi_k^j(b_k^j) - 2\sum_{s=1}^{n/2} \varphi_k^j(b_{k-s}^j)$ *for any k, while $u_*^j(x)$ is the best approximation (16) among all possible Fup coefficients which satisfy (A1). If n = 2, from Eq. (13) or Fig. 3 $r = 26/9 - 2 \times 5/9 = 16/9$ and $1 + 2^n r^{-1} = 52/16$ which means that the FCT has the same order of the approximation as the best possible Fup$_2$ approximation $u_*^j(x)$.*

Difference between FCT and FRT approximation is defined by the following theorem [40]:

Theorem 3. *If $u(x) \in C^{n+2}$, then the following relation is valid:*

$$\|u^j(x) - u_n^j(x)\| = O(\max(\Delta x_j^{n+2}, \Delta y_j^{n+2})) \tag{A4}$$

Therefore, at a sufficiently high level (related to the threshold ε) difference between FCT and FRT should be a quite small. It means that FRT retains good approximation properties of the FCT, but in a more efficient computational way (Eq. (23)).

References

[1] Ababou R, McLaughlin D, Gelhar LW, Thompson AFB. Numerical simulation of three-dimensional saturated flow in randomly heterogeneous porous media. Transport Porous Media 1989;4(6):549–66.
[2] Alturi SN, Shen S. The meshless local Petrov Galerkin (MPLG) method: a simple and less costly alternative to finite element and boundary element methods. CMES: Comput Model Eng Sci 2002;3(1):11–52.
[3] Bakr AA, Gelhar LW, Gutjahr AL, MacMillan JR. Stochastic analyses of spatial variability in subsurface flows: 1. Comparison of one- and three-dimensional flows. Water Resour Res 1978;14(2):263–72.
[4] Bellin A, Salandin P, Rinaldo A. Simulation of dispersion in heterogeneous porous formations: statistics, first order theories, convergence of computations. Water Resour Res 1992;28(9):2211–27.
[5] Bellin A, Rubin Y. HYDRO_GEN: a spatially distributed random field generator for correlated properties. Stochastic Hydrol Hydraul 1996;10(4):253–78.
[6] Cao J, Kitanidis PK. Adaptive grid-simulation of groundwater flow in heterogeneous aquifers. Adv Water Resour 1999;22(7):681–96.
[7] Cliffe KA, Graham IG, Scheichl R, Stals L. Parallel computation of flow in heterogeneous media modeled by mixed finite elements. J Comput Phys 2000;164:258–82. doi:10.1006/jcph.2000.6593.
[8] Cordes C, Kinzelbach W. Continuous groundwater velocity fields and path lines in linear, bilinear, and trilinear finite elements. Water Resour Res 1992;28(11):2903–11.
[9] Cvetković V, Shapiro AM, Dagan G. A solute-flux approach to transport in heterogeneous formations: 2. Uncertainty analysis. Water Resour Res 1992;28(5):1377–88.
[10] Cvetković V, Cheng H, Wen X-H. Analysis of linear effects on tracer migration in heterogeneous aquifers using Lagrangian travel time statistics. Water Resour Res 1996;32(6):1670–1.
[11] Dagan G. Solute transport in heterogeneous porous formations. J Fluid Mech 1984;145:151–77.
[12] Dagan G. Flow and transport in porous formations. Berlin: Springer-Verlag; 1989.
[13] Dagan G, Cvetković V, Shapiro AM. A solute-flux approach to transport in heterogeneous formations: 1. The general framework. Water Resour Res 1992;28(5):1369–76.
[14] Dagan G, Fiori A, Janković I. Flow and transport in highly heterogeneous formations: 1. Conceptual framework and validity of first-order approximations. Water Resour Res 2003;9(9):1268. doi:10.1029/2002WR001717.
[15] Demmy G, Berglund S, Graham W. Injection mode implications for solute transport in porous media: analysis in a stochastic Lagrangian framework. Water Resour Res 1999;35(7):1965–74.
[16] Derfel G, Dyn N, Levin D. Generalized refinement equations and subdivision processes. J Approx Theory 1995;80:272–97.
[17] de Dreuzy JR, Beaudoin A, Erhel J. Asymptotic dispersion in 2D heterogeneous porous media determined by parallel numerical simulations. Water Resour Res 2007;43:W10439. doi:10.1029/2006WR005394.
[18] Dykaar BB, Kitanidis PK. Determination of the effective hydraulic conductivity for heterogeneous porous media using a numerical spectral approach: 1. Method. Water Resour Res 1992;28(4):1155–66.
[19] Ebrahimi F, Sahimi M. Multiresolution wavelet coarsening and analysis of transport in heterogeneous media. Physica A 2002;316:160–88.
[20] Enquist B, Lotstedt P, Runborg O. Multiscale methods in science and engineering. Stockholm: Springer-Verlag; 2003.
[21] Fiori A, Janković I, Dagan G. Flow and transport in highly heterogeneous formations: 2. Semianalytical results for isotropic media. Water Resour Res 2003;39(9):1269. doi:10.1029/2002WR001719.
[22] Frind EO, Matanga BG, Cherry JA. The dual formulation of flow for contaminant transport modeling: 2. The Borden aquifer. Water Resour Res 1985;21(2):170–82.
[23] Gelhar LW, Axness CL. Three-dimensional stochastic analysis of macrodispersion in aquifers. Water Resour Res 1983;19(1):161–80.
[24] Gelhar LW. Stochastic subsurface hydrology. Englewood Cliffs, NJ: Prentice Hall; 1993.
[25] Gotovac B, Kozulić V. On a selection of basis functions in numerical analyses of engineering problems. Int J Eng Model 1999;12(1–4):25–41.
[26] Gotovac B, Kozulić V. Numerical solving the initial value problems by R_{bf} basis functions. Struct Eng Mech 2002;14(3):263–85.

[27] Gotovac H, Andričević R, Gotovac B, Kozulić V, Vranješ M. An improved collocation method for solving the Henry problem. J Contam Hydrol 2003;64:129–49.
[28] Gotovac H, Andričević R, Gotovac B. Multi-resolution adaptive modeling of groundwater flow and transport problems. Adv Water Resour 2007;30(5):1105–26.
[29] Hassan AE, Cushman JH, Delleur JW. A Monte-Carlo assessment of Eulerian flow and transport perturbation models. Water Resour Res 1998;34(5):1143–63.
[30] Hassan AE, Andričević R, Cvetković V. Computational issues in the determination of solute discharge moments and implications or comparison to analytical solutions. Adv Water Resour 2001;24:617–9.
[31] Hou TY, Wu X-H. A multiscale finite element method for elliptic problems in composite materials and porous media. J Comput Phys 1997;134:169–89.
[32] Hsu K-C, Zhang D, Neuman SP. Higher-order effects on flow and transport in randomly heterogeneous porous media. Water Resour Res 1996;32(3):571–82.
[33] Hsu K-C. The influence of the log-conductivity autocovariance structure on macrodispersion coefficients. J Contam Hydrol 2003;65:65–77.
[34] Janković I, Fiori A, Dagan G. Flow and transport in highly heterogeneous formations: 3. Numerical simulation and comparison with theoretical results. Water Resour Res 2003;9(9):1270. doi:10.1029/2002WR001721.
[35] Kansa EJ. Multiquadratics – a scattered data approximation scheme for applications to computational fluid-dynamics: 1. Surface approximations and partial derivative estimates. Comput Math Appl 1990;19(8–9):127–45.
[36] Kolodiazhny VM, Rvachev VA. On the construction of Y. Meyer wavelets using $up(x)$ function. Dop NAN Ukr 1993;(10):18–24.
[37] Kolodiazhny VM, Rvachev VA. Atomic functions: generalization to the multivariable case and promising applications. Cybernet Syst Anal 2007;43(6):893–911.
[38] Kozulić V, Gotovac B. Numerical analysis of 2-D problems using Fup basis functions. Int J Eng Model 2000;13(1–2):7–18.
[39] Kravchenko VF, Rvachev VA. Wavelet systems and their application to signal processing. Foreign Radioelectron: Success Mod Radioelectron 1996;4:3–20.
[40] Kravchenko VF, Basarab MA. Approximations by atomic functions and numerical methods for Fredholm integral equations of the second kind. Differ Eq 2001;37(10):1480–90.
[41] Kravchenko VF. Lectures on the theory of atomic functions and their applications. Moscow: Radiotekhnika; 2003 [in Russian].
[42] Kravchenko VF, Basarab MA, Perez-Meana H. Spectral properties of atomic functions used in digital signal processing. J Commun Technol Electron 2001;46:494–511.
[43] LaBolle EM, Fogg GE, Thompson AFB. Random-walk simulation of transport in heterogeneous porous media: local mass-conservation problem and implementation methods. Water Resour Res 1996;32(3):583–93.
[44] Mallat SG. A theory for multi-resolution signal decomposition: the wavelet representation. IEEE Trans Pattern Anal Mach Intell 1989;2(7):674–93.
[45] Moreno L, Tsang CF. Flow channeling in strongly heterogeneous porous media. A numerical study. Water Resour Res 1994;30(5):1421–30.
[46] Mose R, Siegel P, Ackerer P. Application of the mixed hybrid finite element approximation in a groundwater model: luxury or necessity? Water Resour Res 1994;30:3001–12.
[47] Neuman SP, Zhang Y-K. A quasi-linear theory of non-Fickian and Fickian subsurface dispersion: 1. Theoretical analysis with application to isotropic media. Water Resour Res 1990;26:867–902.
[48] Pollock DW. Semianalytical computation of pathlines for finite difference models. Ground Water 1988;26(6):743–50.
[49] Prenter PM. Splines and variational methods. New York: Wiley; 1989. p. 323.
[50] Rubin Y. Stochastic modeling of macrodispersion in heterogeneous porous media. Water Resour Res 1990;26(1):133–41 [with correction in Water Resour Res 1990;26(10):2631].
[51] Rubin Y. Applied stochastic hydrogeology. New York: Oxford University Press; 2003. p. 391.
[52] Rupert CP, Miller CT. An analysis of polynomial chaos approximations for modeling single-fluid-phase flow in porous medium systems. J Comput Phys 2007;226:2175–205.
[53] Rvachev VL, Rvachev VA. Pro odnu finitnu funkciju. DAN URSR Ser A 1971;6:705–7 [in Russian].
[54] Rvachev VL. Teorija R-funkcij i nekotorija jeje priloženija. Kiev: Naukova dumka; 1982. p. 551 [in Russian].
[55] Saad Y, Schultz MH. GMRES: a generalized minimal residual algorithm for solving nonsymmetric linear systems. SIAM J Sci Stat Comput 1986;7:856–69.
[56] Saad Y. Iterative methods for sparse linear systems. New York: SIAM Journal Press; 2003.
[57] Salandin P, Fiorotto V. Stochastic solute transport in natural formations: finite element and spectral method solution. In: Peters A et al., editors. Proceedings of the X C.M.W.R., vol. 1. Norwell: Kluwer Academic; 1994. p. 571–8.
[58] Salandin P, Fiorotto V. Solute transport in highly heterogeneous aquifers. Water Resour Res 1998;34(5):949–61.
[59] Taylor GI. Diffusion by continuous movements. Proc Lond Math Soc 1921;20:196–212.
[60] Thompson AFB, Gelhar LW. Numerical simulation of solute transport in three-dimensional, randomly heterogeneous porous media. Water Resour Res 1990;126(10):2541–62.
[61] Trefry MG, Ruan FP, McLaughlin D. Numerical simulations of preasymptotic transport in heterogeneous porous media: departures from the Gaussian limit. Water Resour Res 2003;39(3):1063. doi:10.1029/2001WR001101.
[62] Van Lent T, Kitanidis PK. Effects of first order approximations on head and specific discharge covariances in high-contrast log-conductivity. Water Resour Res 1996;32(5):1197–297.
[63] Vasilyev OV, Paolucci SA. A fast adaptive wavelet collocation algorithm for multidimensional PDEs. J Comput Phys 1997;125:16–56.
[64] Vasilyev OV, Bowman C. Second generation wavelet collocation method for the solution of the partial differential equations. J Comput Phys 2000;165:660–93.
[65] Vasilyev OV, Kevlahan N-KR. An adaptive multilevel wavelet collocation method for elliptic problems. J Comput Phys 2005;206:412–31.
[66] Verner JH. Explicit Runge–Kutta methods with estimates of the local truncation error. SIAM J Numer Anal 1978;15:772–90.
[67] Wang R, Keast P, Muir P. A high order global spatially adaptive collocation method for 1-D parabolic PDEs. Appl Numer Math 2004;50:239–60.
[68] Zelkin EG, Kravchenko VF, Basarab MA. Interpolation of signals with a finite spectrum by Fourier transforms of atomic functions and application of this interpolation to antenna synthesis problems. J Commun Technol Electron 2002;47:413–20.